Department of Precision and Microsystems Engineering

Hybrid vibration control with concurrent active piezoelectric and passive viscoelastic damping

Leon Bosscher

Report no : 2022.052
Coach : M.B. Kaczmarek
Professor : Dr. S.H. Hossein Nia Kani
Specialisation : Mechatronic System Design
Type of report : MSc Thesis
Date : 8 September 2022

Delft University of Technology

MSc Thesis: Hybrid vibration control with concurrent active piezoelectric and passive viscoelastic damping

Authors:
L.M.A. Bosscher (4557417)

Supervisors:
Dr. S.H. Hossein Nia Kani
M.B. Kaczmarek

September 8, 2022

Abstract

The use of passive viscoelastic damping and active piezoelectric damping in a hybrid side-by-side configuration is explored in this paper. The goal is to combine the strengths of both individual methods to achieve better damping performance when targeting a single eigenmode or multiple resonances. It is found that a hybrid configuration where a passive constrained layer element covers the strain peak of a mode, with a active element placed next to it performs better than a passive or active damping treatment of the same size. It is more robust and uses lower control gains than active vibration control, and changes the system dynamics less than passive methods.

Acknowledgements

This thesis written to obtain my Master of Science from Delft University of Technology would not have been possible without the support and encouragement I have received from the academic staff, fellow students and my friends and family.

Firstly, I would like to thank Dr. Hassan HosseinNia for providing me with the opportunity to write my thesis under his supervision. He has assisted me in finding inspiration for a research topic and given me invaluable feedback at milestone moments during the year of research.

Secondly, I would like to thank Marcin Kaczmarek, my daily supervisor. The weekly meetings and his support helped me tremendously in completing this thesis. His insights when discussing roadblocks and problems along the way helped me at moments when I felt stuck. He pointed me in the right direction and always encouraged me to look at my work critically.

Finally, I would like to thank my friends, family and girlfriend for their support during this process. Without them, this would have been a lot harder. They were there for me when I needed it most and allowed me to make the most of my time being a student.

Summary

The problem of mechanical vibrations has always presented a challenge to engineers. In the High-Tech industry especially where the operating scales are getting increasingly smaller, damping these vibrations is critical to ensure accuracy and reliability. Viscoelastic materials have proven to be effective, especially in a constrained layer configuration, at damping most vibrations. However, due to their frequency dependent properties, their performance is not consistent. More recent work has dampened vibrations actively with piezoelectric transducers. These are tuned with an active controller to sense and then dampen vibrations. Active damping increases the system complexity and suffers from poor robustness. Both these methods have therefore been combined in a configuration called hybrid vibration control. Numerous configurations of hybrid damping have been studied but a promising and little researched one is where the active and passive elements are used side-by-side.

Previous work at TU Delft by M. Kruik has explored the use of the side-by-side configuration to dampen the first three modes of a beam. In this work separate damping methods were considered for each mode, either active or passive. Furthermore, the frequency dependent characteristics of viscoelastics were not taken into account. This thesis expands the previous work by taking the frequency dependent behavior into account in the model, as well as exploring the simultaneous use of passive and active methods to dampen the same mode. The Ross-Kerwin-Ungar model is implemented into a finite element to represent the complex viscoelastic behavior. This model is then experimentally validated and then used to study various side-by-side hybrid damping configurations.

It is found that partially covering the strain energy peak of a mode with a constrained layer damping patch, and placing a piezoelectric patch of the same length next to it will yield the best damping results. This configuration has the added benefits of lower control gains for the active part, as well as increased robustness were it to fail, being shorter than a purely passive treatment and having less effect on the host structure dynamics. It is also shown that when targeting multiple modes with hybrid damping, many different solutions exist and the best one depends on the requirements for the system.

Contents

Contents iii

I Introduction 1

II Hybrid vibration control with concurrent active piezoelectric and passive viscoelastic damping 6

1 Introduction 7

2 Modelling 8
- 2.1 Beam modelling . . . 8
- 2.2 Viscoelastic modelling . . . 9
  - 2.2.1 RKU model . . . 9
- 2.3 Piezoelectric modelling . . . 10
  - 2.3.1 Actuator & sensor model . . . 10
  - 2.3.2 Active control . . . 10
- 2.4 Validation . . . 11

3 Design considerations for hybrid damping 13
- 3.1 Influence of frequency dependence . . . 13
- 3.2 Parameter influence . . . 13
  - 3.2.1 CLD placement & size . . . 14
  - 3.2.2 PZT size & placement . . . 15
- 3.3 Multiple damping methods for single mode . . . 16
  - 3.3.1 CLD at strain peak . . . 16
  - 3.3.2 PZT at strain peak . . . 17
  - 3.3.3 Shared strain peak . . . 17
  - 3.3.4 Hybrid vs. passive vs. active damping . . . 18
- 3.4 Hybrid damping for multiple modes . . . 19
  - 3.4.1 Influence of single mode hybrid damping on other modes . . . 19
  - 3.4.2 Damping multiple modes . . . 20
  - 3.4.3 Hybrid vs. passive vs. active damping for multiple modes . . . 21

4 Conclusion 21

III Conclusions and recommendations 24

Appendices 30

A Finite element model 31
- A.1 Euler-Bernoulli beam model . . . 31
- A.2 Piezoelectric model . . . 32
- A.3 Viscoelastic model . . . 32
- A.4 System matrix assembly . . . 34
- A.5 Frequency response . . . 34

B Experimental validation 35

B.1 Host structure 35
B.2 Constrained layer damping treatment 35
B.3 Piezoelectric transducers 36
B.4 System Identification 37

C MATLAB code **39**
C.1 FEM model 39
C.2 Calculate element lengths for FEM model 47
C.3 Plotting and results 53

Part I
Introduction

Motivation

Mechanical vibrations have always presented a big challenge to engineers. Whether in terms of structural soundness, performance or simply for user comfort, vibrations can have a detrimental effect on a system [1]. In most cases, the suppression of these vibrations is well studied and a wide variety of solutions are available. The most common method is using viscoelastic materials (VEM), like rubber, to dampen unwanted vibrations. This can be done in several different ways, but the most common and effective is the constrained layer configuration (CLD) [2]. This method is relatively easy to implement and effective at reducing most vibrations, particularly at high frequencies. However, it suffers from poor performance at low frequencies and comes with the cost of added stiffness and mass.

This type of damping might not be sufficient for applications where broadband vibrations are present, due to the poor low-frequency attenuation. Applications in the high-tech industry, where performance requirements are increasingly high and the methods employed - such as vacuum chambers, clean rooms, and lightweight structures - all have very little inherent damping, are one such example. In the semiconductor industry specifically, compliant flexures are used due to their excellent repeatability, accuracy, lack of maintenance and compatability with harsh environments [3]. They are lightweight and stiff and have very little inherent damping. Even the smallest vibrations can cause major problems, if these vibrations are not adequately suppressed, the system performance is compromised and the throughput time increased. The previously mentioned CLD treatment does not always meet the high requirements in these cases, therefore other methods such as active vibration control are employed.

Active vibration control is a potential solution to this challenge. This is most often done with piezoelectric actuators and sensors [4]. Piezoelectrics offer good attenuation at a very large range of frequencies, including the low frequencies where viscoelastic performance suffers. However, this performance comes at the cost of increased system complexity, the need for large control voltages and an external power source and sensitivity to model parameter errors, sensor noise and spillover effects.

Seeing the benefits of these methods, researchers decided to combine them to achieve a hybrid damping system. Hybrid vibration control is the combination of both passive and active techniques and aims to combine the low cost and robustness of passive VEM treatments and the high performance, modal selective and adaptive piezoelectric active control. This could offer a good solution to the high level of damping required in the semiconductor industry. There are many different ways to combine passive and active damping, they are presented and discussed in the following section.

State of the art

The state of the art of hybrid damping is presented in this section. The different possible configurations, challenges that are associated with them and their advantages and drawbacks will be discussed in this section.

An overview of some of the most common configurations of hybrid damping is presented below in figure 1. This is to give a general idea of what is found in literature, there are more possible variations of these configurations. However, they would be too numerous to illustrate and this overview encapsulates the important differences.

The question can then be posed, which one of these configurations is best? Most studies so far have looked into simultaneous action of the passive and active elements; various combinations of constrained layer damping with piezoelectric actuators embedded into the viscoelastic layer or on top of it [5–9]. The most common is a configuration called active constrained layer damping (ACLD). In ACLD, the constraining layer of the viscoelastic is enhanced or replaced with a piezoelectric actuator to increase the shear in the viscoelastic layer and thus increasing the energy dissipation. However, ACLD suffers from a loss in transmissibility due to the actuator having to apply its force through the softer viscoelastic material, this also increases the control gains used.

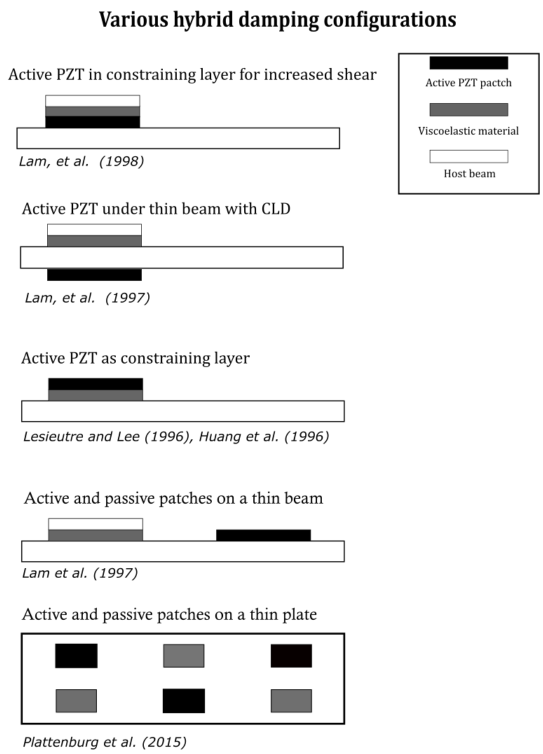

Figure 1: Overview of different hybrid damping configurations

A solution to this problem could simply be using the two different treatments side-by-side instead of stacking them. This was first investigated by Lam et al. [10]. It proved to be a promising alternative, suppressing the vibrations of an impulse faster than other methods, either active or passive, with lower power consumption. The reviews by Benjeddou [8] and Trindade [9] both looked at ACLD and various other configurations and aimed at evaluating their performance. Benjeddou [8] stated it is important to consider the motivation for using hybrid damping in the first place when evaluating its performance. The paper mentions purely active systems require large input voltages and are susceptible to instability from model parameter errors, sensor noise, the actuator/sensor dynamics as well as spillover effects. The addition of viscoelastic damping can help mitigate these effects and generally improve stability. The paper then concludes from numerical studies that configurations in which the active and passive damping treatments act separately have better performance, the configurations from Lam et al. [10] and Plattenburg et al. [11] for example.

Trindade [9] compared the first three different configuration seen in figure 1, he came to the same conclusion as Benjeddou, active and passive treatments used separately tend to perform better. It was also noted that active and passive treatments of different lengths could be used, leading to a reduction in weight.

For the control of these hybrid damping treatments most works made use of simple PD controllers to convey the effectiveness and simplicity of active constrained layer damping [6]. Examples of this are direct velocity feedback and negative velocity feedback, Azvine et al. [5] showed that these could be effective for collocated and non-collocated vibration control. A significant advantage of using hybrid damping is the mitigation of spillover effects. This spillover occurs when a controller of finite dimension is applied to a system with infinite degrees of freedom. This controller cannot account for all the 'residual' modes which can lead to decreased performance or even instability of the system. The addition of a passive element, like VEM, can significantly reduce these effects, as made clear in [12].

Another challenge when designing a hybrid vibration control system and evaluating its damping performance is the modelling. Numerous studies have been carried out, both analytically and numerically, to model viscoelastic and piezoelectric damping. Viscoelastics' damping performance is both temperature- and frequency-dependent, which adds to the complexity of the models. The damping is often characterized through the shear modulus G. This can be chosen as either a a constant or varying with frequency and temperature. Different methods have been developed to represent this shear modulus: the complex modulus, Gollah-Hughes-MacTavish (GHM) or Anaelastic Displacement Field (ADF) method to name a few [13–16]. The easiest way to represent the frequency dependent characteristics is through the complex modulus approach. Here G is expressed as:

$$G^*(j\omega) = G_0(\omega, T)(1 + j\eta(\omega, T)),$$

with the superscript * denoting a complex value, j the imaginary number, ω the frequency, T the temperature and G_0 the storage modulus which is obtained from manufacturer data. The GHM and ADF methods make use of complex series in frequency or s-domain. These last two methods are more difficult to implement and increase the model sizes considerably by adding additional 'dissipation' degrees of freedom. Further model reduction steps are necessary to solve the resulting systems. These methods are more accurate than the complex modulus approach and also allow for time domain information of the system. However, they are far more cumbersome and difficult to implement [17, 18]. For this reason, most studies are limited to one-dimensional beams or thin plates [11] and make use of either the complex modulus approach or a constant shear modulus. This complex modulus approach to represent the VEM behavior can be used with relatively simple models that represent CLD patches such as the Ross-Kerwin-Ungar model. [2].

Optimal size and placement of the damping treatments is also important for performance and has been widely investigated. Optimization heavily depends on the goals and constraints set out by the system designers, such as maximizing damping ratios, minimizing added weight or minimizing control gains. For placement, most studies find that the damping treatments should be placed on the points of maximum strain. However, when aiming to control multiple modes with a limited amount of added weight, this can be challenging [19–22]. Lam et al. [10] used linear quadratic regulator (LQR) to determine the optimal location of the treatment as well as the optimal control effort. Baz et al. [6] first looked at optimal thickness of the viscoelastic layer and optimal control gains. Kruik [23] aimed at optimizing the location of active and passive damping on a dimensional structure by selecting one method for each mode to be damped.

Problem definition

Previous works have shown the side-by-side configuration of hybrid vibration control to be the most promising. These works have shown that it performs better than ACLD and improves the robustness of the system.

The design of such a system presents a challenge. The many variables present make finding an optimal setup difficult. The size and placement of the passive and active components determine in large part the performance, placing the damping treatment at the point of maximum strain usually results in the best performance. However, when faced with multiple modes to damp and either passive or active damping, the choice of placement is not trivial. Furthermore, one wishes not to add too much mass to a system as to significantly alter its dynamics.

A previous study has attempted to find a strategy to find an optimal configuration when designing a system with hybrid damping [23]. However, this work only considered one method of damping per eigenmode. To achieve better performance, it might be beneficial to use both active and passive methods to dampen the same mode. Furthermore, this study ignored the complex frequency dependent behavior of viscoelastics. This can substantially impact the accuracy of the final result, as will be shown in this report.

Research goal & objectives

The research will focus on improving previous work on the design of optimal side-by-side hybrid damping. The main research objective can be defined as:

Develop a design methodology for side-by-side hybrid damping by considering complex viscoelastic properties and simultaneous use of active and passive methods for the same eigenmode.

This goal will be achieved by realizing the following objectives:

1. **Improving the viscoelastic model.** The model used to describe viscoelastic behavior should include the frequency dependence. This should be done in a way that is as straightforward as possible to reduce modelling complexity when designing a hybrid damped system. The Ross-Kerwin-Ungar model with a complex shear modulus for CLD beams is implemented in this work, due to its relative simplicity and inclusion of frequency dependence.
2. **Investigate parameter influence.** Different parameters such as the length, height, thickness and placement of the damping patches have a big effect on their performance. The influence of these on the damping performance will be investigated. This is done by individually looking at the effect of each of these parameters on the damping ratio of an eigenmode of the system. First the placement of the individual methods will be investigated, once the optimal placement is found the influence of other parameters will be taken into account.
3. **Study use of damping methods individually and together when targeting the same mode.** Previously, only one method, either passive or active, was used to suppress a target eigenmode. However, by simultaneously using passive and active methods to target the same eigenmode, superior performance could potentially be achieved. The performance of using an individual damping method will be compared to using both methods simultaneously. The individual patch will be replaced with a hybrid treatment of the same size and at the same location to ensure a fair comparison. The effect on damping performance will be evaluated, as well as changes in system dynamics, control gains and robustness.

Thesis outline

This thesis is presented in paper format in part II. The problem is briefly introduced then the modelling is discussed. The results are then presented and recommendations are given for the design of hybrid damped system, for single and multimode damping. In part III conclusions are drawn from the results of the paper with respect to the goals set out in the introduction. Finally recommendations are given to improve the results and further explore the field of hybrid vibration damping. Appendix A gives a detailed look at the model, appendix B explains the experimental setup and appendix C presents the MATLAB code which was used to model the system.

Part II

Hybrid vibration control with concurrent active piezoelectric and passive viscoelastic damping

Hybrid vibration control with concurrent active piezoelectric and passive viscoelastic damping

***Abstract* - The use of passive viscoelastic damping and active piezoelectric damping in a hybrid side-by-side configuration is explored in this paper. The goal is to combine the strengths of both individual methods to achieve better damping performance when targeting a single eigenmode or multiple resonances. The hybrid method performs better than a passive or active damping treatment of the same size. It is more robust and uses lower control gains than active vibration control, and changes the system dynamics less than passive methods.**

1 Introduction

The problem of vibrations has always presented a challenge to engineers. Whether in terms of structural soundness, performance of simply user comfort, these vibrations can have a detrimental effect on a system. The most common method to combat these vibrations is with the use of viscoelastic materials (VEM). This has been well studied in the past and is a simple and effective solution. These are often used in a sandwich configuration known as constrained layer damping (CLD) [2]. This increases the shear in the viscoelastic and allowing it to dissipate more energy. Modelling these materials' frequency dependent damping characteristics has produced different methods to accurately capture these properties. A frequency domain approach is the easiest way to construct a model for VEM [24]. Time domain approaches also exist but are more complex to implement [14]. The main drawbacks of using VEM and CLD is the mass and stiffness they add to the system, and their poor performance at low frequencies.

The most recent development is the use of piezoelectric transducers (PZT) as actuators and sensors with a control loop to actively suppress vibrations [4]. PZTs offer good vibration attenuation at low as well as high frequencies and can be tuned to specific requirements. However, they are much more complex to implement than VEM, they require large control voltages and are sensitive to variations, sensor noise and spillover effects [25].

The advantages that both the previously mentioned methods have been combined in what is known as hybrid active-passive vibration control. This combines passive viscoelastic damping with active piezoelectric damping. There are many different possible configurations, each with their benefits and drawbacks. Active constrained layer damping (ACLD) has been largely researched [6, 18, 26]. This places a PZT on top of the CLD treatment, either replacing or enhancing the constraining layer. The main idea is to increase the shear in the VEM to dissipate more energy. However, this requires high control voltages for the PZT because it has to act through the VEM layer.

Researchers found that the configuration where the viscoelastic and piezoelectric elements are used concurrently in a side-by-side configuration performs better than ACLD [14, 27]. This has the advantages of lower control voltages for the active PZT, resulting in increased controller stability. Another advantage is the robustness that the viscoelastic adds to the system. It would ensure that in the event that the active control fails or becomes detuned, there would still be damping present. Despite this method being a promising way to combine active and passive vibration control, it is still not yet well researched.

Previous work by Kruik [23] has developed a simple method to aid the design of a hybrid damping system. However, this method lacks certain important aspects of VEM modelling and only considers one method of damping per mode. Modelling VEM is challenging due to its complex frequency dependent behavior. Researchers often chose to ignore this or implement cumbersome methods to represent this.

The models that can most accurately represent VEM's are the Gollah-Hughes-MacTavish (GHM) [13] method and the Anaelastic Displacement Fields (ADF) [16] method. These are used in conjunction with finite element models and add additional dissipation degrees of freedom to the model. This results in increasing model sizes, that require additional model reduction steps to be solved [14]. To avoid these convoluted methods, a different method was employed in this paper, one which can be easily implemented yet still captures the frequency dependent behavior know as the Ross-Kerwin-Ungar method [2]. Finding a simple and reliable method and certain rules of thumb to add damping to a system could greatly simplify and expedite the design process.

This paper aims to investigate the use of both active and passive methods to suppress the same mode. In section 2 a simple model is presented that captures the frequency dependent characteristic of VEM. Then the modelling of PZT and the tuning of the controller is discussed. The model is then validated with an experiment. Section 3 explores different ways of combining active and passive damping, first for the same mode and then for multiple modes. Finally recommendations are given to aide the design of added damping onto a system.

2 Modelling

A model is used in this paper to determine the performance of the damped system. First the host structure is modelled using the Euler-Bernoulli approach. Then the Ross-Kerwin-Ungar (RKU) was selected to model the CLD elements because of its relative simplicity and ability to capture VEM frequency dependence. The modelling of active piezoelectric damping is then presented. Finally the model is experimentally validated.

2.1 Beam modelling

The base beam structure is modelled using Euler-Bernoulli beam elements. This is a simple method to represent linear elastic beams. This model assumes a one dimensional slender beam, with small deflections and only lateral loads. The choice was made for this model because it can be combined with models for the passive and active damping elements and despite its simplicity, it provides enough insight to determine the performance of a damped beam.

A beam element has length L and has four degrees of freedom, two lateral displacements and two rotations:

$$\mathbf{u}_e = [w_1, \theta_1, w_2, \theta_2]. \tag{2.1}$$

Each element has its own 4 by 4 stiffness and mass matrix. These can be used in the equations of motion to derive the dynamics of the system. The stiffness and mass matrix are described as follows [28]:

$$\mathbf{K}_e = \frac{EI}{L^3}\begin{bmatrix} 12 & 6L & -12 & 6L \\ 6L & 4L^2 & -6L & 2L^2 \\ -12 & -6L & 12 & -6L \\ 6L & 2L^2 & -6L & 4L^2 \end{bmatrix} \tag{2.2}$$

$$\mathbf{M}_e = \frac{\rho AL}{420}\begin{bmatrix} 156 & 22L & 54 & -13L \\ 22L & 4L^2 & 13L & -3L^2 \\ 54 & 13L & 156 & -22L \\ -13L & -3L^2 & -22L & 4L^2 \end{bmatrix}. \tag{2.3}$$

However, since the system is comprised of multiple elements, these matrices need to be combined by coupling the nodal degrees of freedom of each element, this is descried in appendix A.4. Once this is done the equation of motion of the whole beam can be written as:

$$\mathbf{M}_{sys}\ddot{\mathbf{u}} + \mathbf{K}_{sys}\mathbf{u} = \mathbf{F}_{ext}. \tag{2.4}$$

Finally, appropriate boundary conditions need to be applied to make the system solvable. The beam is clamped at one end, this is done by setting the degrees of freedom of the clamped node to zero.

2.2 Viscoelastic modelling

2.2.1 RKU model

The viscoelastic elements are modelled using the Ross-Kerwin-Ungar (RKU) method [2]. This method was one of the first to accurately model a three layer sandwich beam with a viscoelastic core. This model is chosen due to its relative simplicity and its inclusion of frequency dependent behavior. It assumes that only the middle layer (VEM) is subject to shear distortion. The base beam and constraining layer are only subjected to bending. The model calculates a complex stiffness EI^* of the constrained layer damping (CLD) element.

$$EI^* = E_1(\frac{H_1^3}{12} + H_1D^2) + E_2^*(\frac{H_2^3}{12}H + H_2(H_{21} - D^2)) + E_3(\frac{H_3^3}{12} + H_3(H_{31} - D^2)) - E_2^*\frac{H_2^2}{12}(\frac{H_{31} - D}{1+g}) - [\frac{E_2^*H_2}{2}(H_{21} - D) + E_3H_3 (H_{31} - D)](\frac{H_{31} - D}{1+g}) \tag{2.5}$$

with the following parameters depending on material and geometric properties.

$$D = \frac{E_2^*H_2(H_{31} - \frac{H_{21}}{2})g(E_2^*H_2H_{21} + E_3H_3H_{31})}{E_1H_1 + \frac{E_2^*H_2}{2}g(E_1H_1 + E_2^*H_2 + E_3H_3)} \tag{2.6}$$

$$g = \frac{G_2^*}{E_3H_2H_3p^2} \tag{2.7}$$

$$H_{21} = \frac{H_1 + H_2}{2} \tag{2.8}$$

$$H_{31} = \frac{H_1 + H_3}{2} + H_2. \tag{2.9}$$

This stiffness EI^* is complex due to the the complex Young's modulus E_2 of the VEM layer. This stiffness changes with frequency and is calculated from the complex shear modulus G^* of the VEM.

$$E^*(j\omega) = 2(1+\nu_v)G^{'}(j\omega), \tag{2.10}$$

$$G^*(j\omega) = G^{'}(\omega)[1 + j\eta(\omega)] \tag{2.11}$$

The shear modulus and Poisson ratio ν_v is obtained from the manufacturer of the damping tape. Values of the storage modulus $G^{'}$ and loss factor η are provided at discrete points over a frequency range and constant temperature in a nomograph and can then be interpolated at different frequencies within the provided range. In this case the range is between 0.1 and 1000 Hz and values are selected at room temperature.

The CLD element can be included in the larger FEM model simply by changing the term EI from (2.2) to the new complex stiffness EI^*. However, since the stiffness changes with frequency the equation of motion needs to be transformed into frequency domain and it needs to be evaluated at each frequency of interest.

$$[-\omega^2\mathbf{M} + \mathbf{K}(j\omega)]\mathbf{U}(j\omega) = \mathbf{F}(j\omega) \tag{2.12}$$

The following process is repeated for each frequency ω_i and the EoM is solved for $\mathbf{U}(j\omega)$ and from this, a transfer function can be calculated between a harmonic force input F_i at the i^{th} DoF and displacement output at the o^{th} DoF $H_{oi}(j\omega) = \frac{\mathbf{U_o}(j\omega)}{\mathbf{F_i}}$.

To determine the damping performance of the CLD patch, the damping ratio is calculated. This is done through the strain energy method. First, the strain energy distribution throughout the entire system is calculated at a given resonance frequency. This is made up of the energies in the base beam and the viscoelastic layer. Due to the segmentation of the beam into finite elements, this calculation is done per element n:

$$U_b^n = \frac{1}{2}\bar{u}^n\mathbf{K}_b(\bar{u}^n)^T \tag{2.13}$$

$$U_v^n = \frac{1}{2}\bar{u}^n\mathbf{K}_v(\bar{u}^n)^T. \tag{2.14}$$

$\bar{u}^n$ represents the displacement of the element, $\mathbf{K}_b$ and $\mathbf{K}_v$ are the beam and CLD stiffness matrices respectively. The system loss factor η can be calculated by dividing the dissipated strain energy by the total strain energy. The damping ratio ζ finally is defined as half the loss factor.

$$\eta = \sum_{i=1}^{n} \frac{U_v^n \eta_v}{U_b^n + U_b^n} \quad (2.15)$$

$$\zeta = \frac{1}{2}\eta. \quad (2.16)$$

2.3 Piezoelectric modelling

2.3.1 Actuator & sensor model

The piezoelectric transducers are included in the finite element model using the method described by Aktas [29]. This model can be readily combined with the Euler-Bernoulli beam model as well as the RKU CLD model. Similarly to how the RKU model returns a stiffness and mass for the CLD element, this model returns the same for an active piezoelectric element. This can then be added to the total stiffness and mass of the system. The piezoelectric element is made up of two transducers, on the top and bottom of the beam, one acting as an actuator and the other as a sensor.

The aforementioned dual use of PZTs is known as the piezoelectric effect. This entails that when a voltage is applied, the PZT experiences a strain. The opposite is also true, when a strain is applied to the transducer, a voltage is generated. The constitutive equations of piezoelectrics that describe this behavior are shown below:

$$\varepsilon_x = S_{11}^E \sigma_x + d_{31} E_z \quad (2.17)$$

$$D_z = d_{31}\sigma_x + \xi_{33}^{\sigma} E_z, \quad (2.18)$$

where ε_x, S_{11}, σ, d_{31}, E_z, D_z and ξ_{33} represent the strain, compliance, stress, piezoelectric strain constant, electric field, electric displacement and permittivity respectfully.
Equation 2.18 expresses the direct piezoelectric effect and is used to determine the total charge generated in the piezoelectric sensor. This charge can be converted into a current and from that the strain can be calculated. The current is converted into a voltage that can be used in a control loop

$$V^s(t) = Hze_{31}w \int_0^{l_p} n_2 \dot{u} dx = S\dot{u}, \quad (2.19)$$

where H is the signal conditioning device gain, z the distance to the neutral axis, e_{31} is the piezoelectric stress constant, w the width of the sensor, l_p the length of the sensor and n_2 the second spatial derivative of the shape function. This sensor voltage can be multiplied with a control gain and fed as an input into the actuator. Subsequently the actuator voltage results in a bending moment and a force being applied onto the beam. The bending moment can be found with:

$$M_{act} = E_p d_{31} \bar{z} g V^s, \quad (2.20)$$

with E_p being the Young's Modulus of the piezoelectric patch, $\bar{z}$ is the distance to the neutral axis and g a control gain. The force that is applied onto the beam is described by the following:

$$f_{act} = E_p d_{31} w \bar{z} (gV^s) \int_0^{l_p} n_1^T dx. \quad (2.21)$$

This force can be included in the general equation of motion as follows:

$$\mathbf{M}\ddot{u} + \mathbf{K}u = F_{ext} + F_{act}. \quad (2.22)$$

2.3.2 Active control

To use the piezotransducers for the intended goal of active vibration control (AVC), a controller needs to be implemented into the control loop. The sensor measures a strain and converts it into a voltage which is sent to the controller. The controller then outputs a voltage to the actuator which results in a force being applied onto the host structure, an block diagram of this loop is shown in figure 2. A relatively simple control algorithm is implemented, Positive Position Feedback (PPF) because it shows good performance for AVC [30], global stability conditions that are easy to satisfy [31]. Other more complex control strategies are also available, but the choice was made to use a simple strategy to showcase a general case.

PPF can be tuned to target one specific eigenmode of a system. It has low pass behavior and adds flexibility to the system at frequencies below its cut-off. At high frequencies it adds stiffness, however this addition is small due to the controller's roll-off. The closed loop diagram is shown in figure 2. The controller's transfer function is given in (2.23). k is the controller gain, ω_c represents the cut-off frequency of the controller and ζ_c is the controller's damping ratio.

$$G(s) = \frac{k\omega_c^2}{s^2 + 2\zeta_c\omega_c s + \omega_c^2}. \tag{2.23}$$

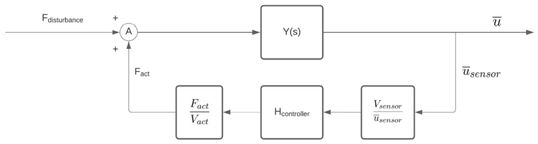

Figure 2: Schematic for closed loop AVC [23]

Different methods exist for finding the optimal controller values. General rules of thumb can be found, suggesting a cut-off frequency between 1.3 to 1.45 times the natural frequency, and a damping ratio between 0.1 and 0.5 [32, 33]. ζ_c has a large influence on the performance of the controller. When it is small, the resonance peak of the controller is higher, meaning the actuator exerts more force onto the system. However the slope of the phase angle is very steep which implies that the system is not very robust, meaning that if the controller performs worse if the calculated natural frequency deviates from the actual natural frequency [34]. Other more complex methods exist to find the optimal parameters [35, 36]. However, for the purpose of this study, using the rules of thumb was sufficient. The gain of the controller determines the stability of the system with the following condition [30]:

$$0 < kG(0) < 1. \tag{2.24}$$

The gain and damping ratio of the controller can be selected using the conditions stated above and by observing whether the targeted resonance peak is sufficiently damped [37].

The damping performance of the active system is done by calculating the Q factor, which is defined as the energy stored over the energy supplied at resonance. This is a simple method from which the damping ratio can be calculated. The Q factor is calculated using the frequency response function of the closed-loop system and a 3dB gain margin [38].

$$Q = \frac{f_0}{\Delta f_{3dB}} \tag{2.25}$$

$$\zeta = \frac{1}{2Q}. \tag{2.26}$$

Here f_0 is the center frequency, or resonance frequency and Δf_{3dB} is the 3dB bandwidth around the resonance peak.

2.4 Validation

An experiment is carried out to validate the model used. This is important to determine the reliability of the model when using it for design purposes.
An aluminium beam is used as the base structure with 3M 2552 damping foil as the CLD treatment. The beam is vertically oriented.

Beam parameters	
Length (m)	0.277
Height (m)	0.0015
Width (m)	0.04
Young's Modulus (GPa)	70
Density (kg/m^3)	2700

Table 1: Beam parameters

Table 1 shows the parameters of the base beam. The beam is clamped at one end. A disturbance input is provided at near the base of the beam and the strain is measured at the same location. Two PI P876-A12 piezoelectric transducers are placed on each side of the beam near the base, 1 cm above the clamped end. This location is chosen because it experiences high strain for multiple bending modes. One of these collocated transducers provides the force disturbance input and the other functions as a sensor that provides a signal proportional to the strain of the patch, which is used as a generalized position measurement.

The setup uses a TI LAUNCHXL-F28379D micro-controller to send the disturbance signal to the actuator as well as to measure the signal coming from the sensor. The actuator disturbance signal is sent through a BD300 voltage amplifier to deliver adequately high voltage to drive the transducer. The sensor signal is sent through a charge amplifier circuit to convert the charge signal into a voltage signal and to condition the input to the analog-to-digital converter [39].

Code is written and generated in MATLAB Simulink to send a chirp signal from 1 to 1000 Hz to the actuator for system identification. Data is logged with Simulink and then manipulated in MATLAB. A transfer function can be calculated between the collocated force input and strain measurement. The frequency response is generated using the *tfestimate* function.

Two experiments are carried out to validate the model. One where the beam aluminium beam is bare except for the piezoelectric transducers near the base. The second has a 10 cm and 4 cm wide strip of 3M 2552 damping foil placed above the transducer, 7.5 cm above the base of the beam. This location is chosen because of its high strain, especially for the second eigenmode. The frequency response from the experiment of the damped and undamped beams is shown in figure 3. The results are then compared with the model in table 2.

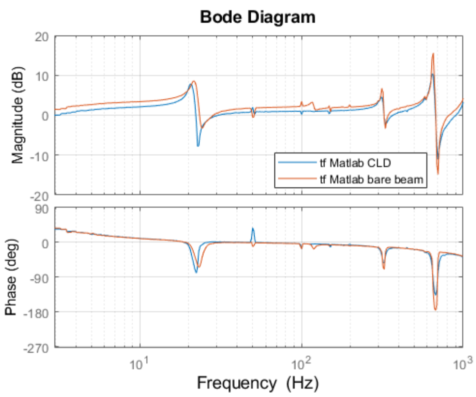

Figure 3: Experimental FRF of damped and undamped beam

The results presented in table 2 show relatively good agreement between the model and the experimental results. A difference is the shift in eigenfrequencies, in the model a clear shift higher can be seen when damping tape is added. This is due to the added stiffness of the constraining layer and viscoelastic layer. However, the experiment doesn't reflect this behavior. This could be because the RKU model overestimates the stiffness added by the CLD tape, or it could come from a mismatch in the properties of the damping tape. At low and high frequencies this difference is relatively small, with a maximum difference of 9% for the undamped 4^{th} eigenmode.

Experiment

Mode	Undamped	Damped
1	21.7 Hz	20.3 Hz
2	111 Hz	-
3	319 Hz	319 Hz
4	634 Hz	634 Hz

Simulation

Mode	Undamped	Damped
1	21.7 Hz	23.9 Hz
2	110 Hz	130 Hz
3	297 Hz	311 Hz
4	594 Hz	690 Hz

Table 2: Eigenfrequencies of experiment vs simulation

A further difference between the model and experiment is the second mode of the beam. In the undamped case, this mode is only barely visible in the bode plot and when damping is introduced this mode is no longer visible. This can easily be explained by looking at the strain energy of the second mode and observing that the sensor is placed where the energy is minimal, see figure 6, thus rendering this mode unobservable. For the other modes the damping ratio is compared between the experiment and model.

Mode	Experimental ζ	Numerical ζ
1	0.05	0.07
3	0.07	0.08
4	0.03	0.09

Table 3: Experimental vs numerical damping ratio

These results shown in table 3 show good agreement between experiment and model. The differences are small and are most likely due to a difference in the properties of viscoelastic material from the experiment versus the data from the manufacturer used in the model. Another contributing factor is the model not including any inherent damping in the bare beam.

The model provides sufficient insight into the damping behavior of viscoelastic materials and can be useful when designing a system that needs to be damped.

3 Design considerations for hybrid damping

The influence of different parameters are investigated, for the purely passive, purely active and hybrid configurations. First the influence of VEM frequency dependence of the model is evaluated. Then the influence of size and placement of the passive damping patch is investigated. This is repeated for the active and hybrid cases. The use of active, passive and hybrid methods are compared when damping a single mode and conclusions are drawn about the most effective method. Finally, the influence of hybrid damping on other modes is investigated and suggestions are given when damping multiple modes.

3.1 Influence of frequency dependence

As mentioned in 2.2, viscoelastics exhibit frequency dependent behavior. The shear modulus and loss factor change with frequency. This can be seen in the nomograph provided by the manufacturers of VEM damping treatments, see figure 4.

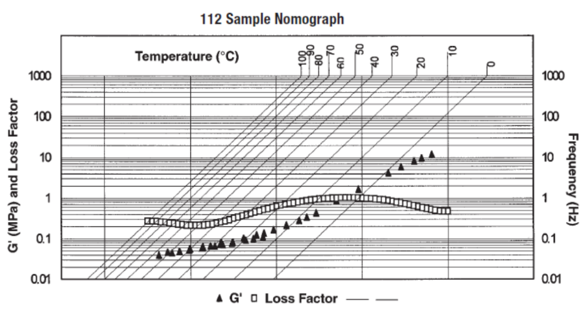

Figure 4: Nomograph for 3M ISD122 damping tape

To investigate the frequency dependence, the damping ratio for the first 4 eigenmodes of the beam from 2.4 is calculated. First with constant shear modulus G^* taken from the nomograph at 1 Hz and 10 Hz, then with a varying G^* across the entire frequency range. The results are presented in table 4.

Mode	ζ G^* @1Hz	ζ G^* @10Hz	ζ varying G^*
1	0.014	0.029	0.037
2	0.079	0.175	0.182
3	0.024	0.050	0.052
4	0.073	0.187	0.142

Table 4: Effect of frequency dependence on damping ratio for first four eigenmodes

The results indicate that depending on the value of the shear modulus, the damping ratio varies greatly. These results are illustrated in figure 5, showing the frequency response of a beam with CLD treatment with either constant or varying G^*. Using a constant G^* yields very different results than when using a varying G^*, with the height of the resonance peaks varying. Therefore to more accurately capture the behavior of viscoelastics it is better to include this frequency dependence. Furthermore, the changing the shear modulus also affects the stiffness matrix of the system, leading to a shift in the eigenfrequencies when compared to a constant G^*. However, the shift observed in figure 5 is relatively small, the first mode has no observable change and subsequent modes differ only by a maximum of 3 Hz at low frequencies and 20 Hz at high frequencies.

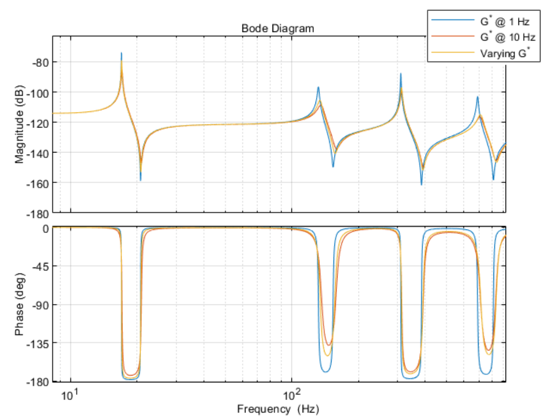

Figure 5: FRF of CLD beam with varying G^*

3.2 Parameter influence

The influence of various parameters such as size and placement of individual damping treatments on performance are investigated in this section. This will give insight into the configuration which adds the most damping and will be useful when considering both methods together.

3.2.1 CLD placement & size

The placement and size of the damping treatment determines in large part its performance. Even the most effective damping treatment placed at the wrong location on the system will deliver poor results. It has been well established that the CLD patch has to be placed at the location of maximum strain for it to be most effective. The strain energy distribution of the 2^{nd} eigenmode best illustrates this since it has a clear peak. The peak is centered around the middle of the beam as seen in figure 6. A CLD patch covering 36 % of the beam is placed at different locations along the beam and the damping ratio is calculated at each of these locations. The results are presented below in table 5:

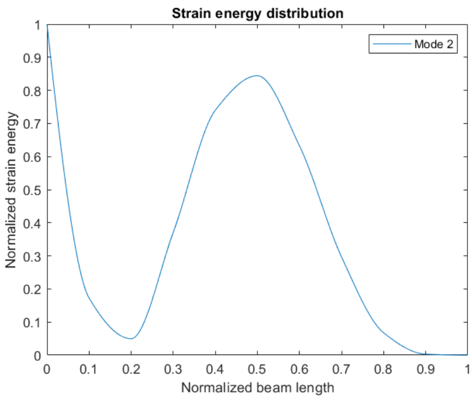

(a) Strain energy distribution of 2^{nd} eigenmode

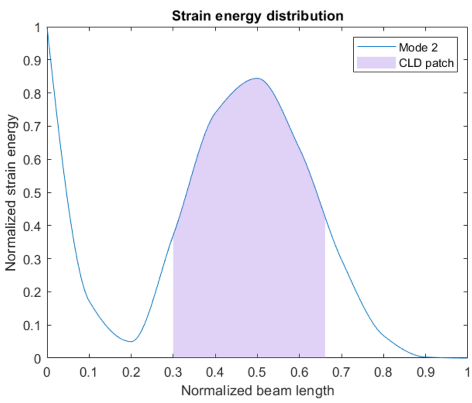

(b) Optimal CLD patch location for 2^{nd} eigenmode

Figure 6: Strain energy of 2^{nd} eigenmode

These results illustrate the importance of placing the damping patch at the location of maximum strain of the beam. When the CLD patch is placed at 0.3L and is then centered around the strain energy peak, as seen in figure 9b, the VEM layer experiences the biggest shear and can thus dissipate the most energy. This will dampen the mode of interest the most, as can be seen from the results in table 5.

The size of the patch also has an influence on the damping performance. The influence of length, VEM height and constraining layer height are investigated for the second eigenmode. The patch is centered around the strain energy peak.

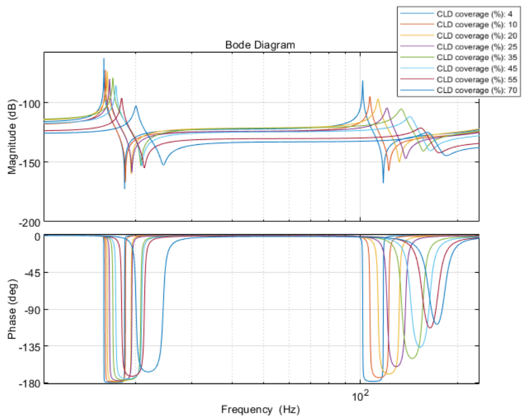

Figure 7: Frequency response with varying CLD coverage

It is evident from the results in table 5 and figure 7 that the more the beam is covered, the higher the modal damping ratio, this is true for all modes. Furthermore, figure 7 shows the frequency response of the CLD covered beams. It can be observed that with increasing coverage, the eigenfrequencies shift higher. This is due to the stiffness that the CLD treatment adds. Aside from stiffness, the CLD treatment also adds mass. This might not always be desirable, depending on the design requirements. Therefore compromises need to made when choosing the length of CLD to be added onto the beam and it is high dependable on the situation.

Position ($\frac{x}{L}$)	ζ	**Length (%)**	ζ
0.01	0.04	5	0.01
0.1	0.04	10	0.04
0.2	0.12	20	0.07
0.3	0.18	25	0.11
0.4	0.15	35	0.18
0.5	0.08	55	0.29
0.6	0.04	70	0.31

Table 5: Effect of CLD position and length on damping ratio of 2^{nd} eigenmode

The influence of height of the VEM and constraining layer is more complex. Damping performance can be characterized by the deformation of the viscoelastic material, the more shear, the more energy gets dissipated and thus the higher the damping in the system. According to the RKU model the loss factor can be calculated by the following [40]:

$$\eta = \frac{2\pi}{3}\frac{G''}{E}\frac{L^2}{th} \tag{3.1}$$

with G'' being the shear loss factor of the VEM at a given frequency, E the elasticity modulus of the VEM and t and h the thickness of the VEM and constraining layers respectively. This formula implies that the loss factor can be made large by making the VEM treatment as thin as possible, this is consistent with the findings of Lam et al. [10] and Nashif et al. [41]. However, this is not always realistic. If the shear strain is made arbitrarily large by making the layers very thin, the shear stress would damage the VEM and constraining layer. Nonetheless, this model serves well to demonstrate the effectiveness of the shear mechanism and gives insight into the damping performance. Furthermore, the height of the damping tape is one of the parameters that not always adjustable, as the CLD is delivered as a roll of tape by the manufacturer. The length is therefore easily adjusted, whereas the thickness is set depending on the type of CLD tape. For the purpose of this design study, the dimensions of commercially available 3M ISD122 Damping Tape are taken, with a VEM thickness of 0.127 mm and a constraining layer that is twice as thick.

3.2.2 PZT size & placement

Equally as important as the placement and size of the CLD patches is that of the active piezoelectric patches. As was done in the previous section for passive damping, first the effect of location is investigated, then the length of the treatment is varied and its influence studied.
It is also well established that for active damping to be effective, it should be placed in location of maximum strain. This was confirmed in the numerical model by placing a 6 cm long piezoelectric patch pair, modelled after a PI-876.A12 transducer, at different points along the beam. The controller is tuned to the 2^{nd} mode. Tuning of the parameters was done by performing a sweep with integer values for the gain k ranging from 1 to 5 and doubles with an accuracy of 0.10 for the damping ratio ζ_c ranging from 0.1 to 0.5, according to the rules of thumb discussed in section 2.3.2 The parameters are left the same for the subsequent tests. Then the damping ratio is calculated to evaluate the performance.

Position ($\frac{x}{L}$)	**Damping ratio** ζ
0.05	0.03
0.1	0.01
0.2	0.03
0.3	0.09
0.4	0.19
0.5	0.13
0.6	0.06

Table 6: Damping ratio of 2^{nd} mode as function of PZT position

It can be seen in table 6 that when the actuator/sensor pair is placed at $\frac{x}{L} = 0.4$, which centers it at the strain peak (see figure 6), the best performance is achieved. This is in line with expectations, therefore a active damping patch should be placed at the strain peak to achieve the best performance.

Next the length of the PZT patch is varied and its effect studied. The patch is placed in the center of the strain peak of the second eigenmode. The length of the patch is expressed as a percentage of the beam that it covers. The damping ratio is given as well as the eigenfrequency, since it tends to shift due to the added stiffness.

The results in figure 8 show that with increasing coverage, the damping performance increases as well. In the case where the beam is 50 % covered, thus when the strain peak is fully covered (see figure 6), the resonance peak is suppressed the most. The damping ratio ζ reaches 0.51 versus the 0.03 when the beam is only covered by 10 %. The eigenfrequency is also shifted up due to the added stiffness of the PZTs. On the other hand, the frequency of the first mode is shifted lower due to the flexibility that the controller adds. When the beam is covered by 50 % the shift is -30 %. Covering half the structure or more is also not always practical. Similarly to the case with passive damping, this adds mass and stiffness to the host structure, changing its dynamics. The choice of length of the actuator depends on the design requirements and should be carefully considered.

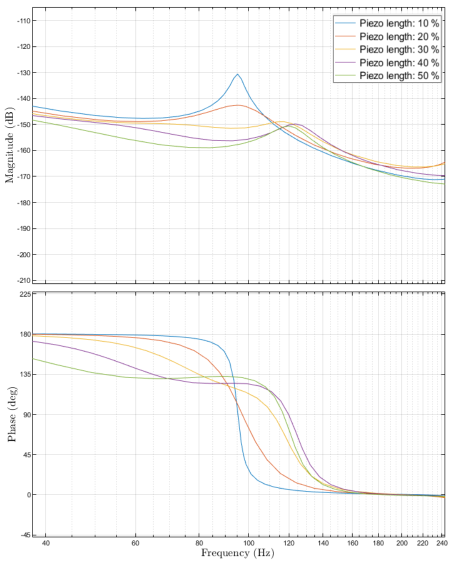

Figure 8: 2^{nd} mode damping with varying PZT length

Finally, as seen in 2.3.2, the damping performance also depends on the controller parameters. If the gain is increased, more damping can be added. There are limits to this gain however, based on controller stability and hardware limitations.

3.3 Multiple damping methods for single mode

Now that the passive and active methods have been studied individually, the use of them side-by-side is explored. In this paper both methods are combined to dampen the same mode. The reason for this is to achieve better performance than when using just one method, as well as making the system more robust were the active component to fail.

3.3.1 CLD at strain peak

The first configuration is a CLD patch of 15 % of the beam length centered around the strain peak for the 2^{nd} mode. The position of the active patch is varied around this strain peak and the influence investigated. It is first placed near the base of the beam and incrementally moved closer to the passive patch. The controller is tuned again using the rules of thumb, for an ideal case where the PZT is at the strain peak, they are kept the same for each iteration in this section. They are later tuned for optimal performance when an ideal configuration is found. It is found that when the two treatments are placed right next to each other, the best damping performance is achieved, see table 7. This configuration is also illustrated in figure 9.

Position ($\frac{x}{L}$)	ζ	f_n
0.01	0.06	120
0.075	0.07	113
0.1	0.08	112
0.15	0.07	108
0.20	0.07	107
0.25	0.12	98.2
0.3	0.13	98.5
0.325	0.14	98.3

Table 7: Hybrid damping performance with varying piezo placement

This can be attributed to the fact that they are covering the highest amount of strain energy, and as seen in sections 3.2.1 and 3.2.2 this is the most important factor when determining the placement of the patches. Furthermore, the damping performance achieved in this configuration is improved by a factor 6 when compared to using an active patch of similar dimensions and also 28 % better than when using pure passive damping. Next, it can be observed that the eigenfrequency shifts as a function of the placement. Adding damping to the system tends to increase the eigenfrequency, due to the added stiffness. However, the controller also has an influence. When the active patch is placed at a location of higher strain this tends to decrease the resonant frequency. This needs to be considered when designing a hybrid damping system.

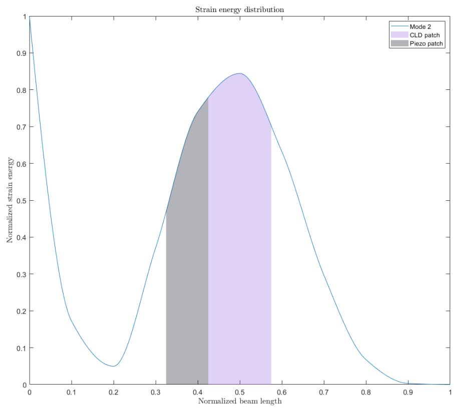

(a) Strain energy distribution of 2^{nd} eigenmode with CLD at peak

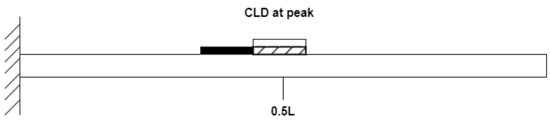

(b) Schematic of beam with CLD at peak and PZT at optimal location

Figure 9: CLD at peak with PZT at optimal location

Finally, the robustness of the system is considered. Due to the presence of passive damping, if the active component were to fail, the beam would still have some measure of vibration suppression. In the case where the PZT is placed against the CLD patch, the damping ratio for the 2^{nd} mode would be 0.07. This acts as a good redundancy for the worst case scenario.

3.3.2 PZT at strain peak

The same process is repeated for a active PZT patch centered around the strain peak of the 2^{nd} eigenmode. Patches of the same dimensions are used. Again the controller parameters are kept the same. The results are presented below in table 8 and illustrated in figure 10.

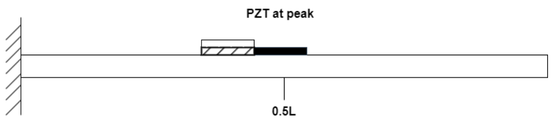

Figure 10: PZT at peak with CLD at optimal location

The same conclusions can be drawn as in the previous section. Both damping treatments need to be placed as close to each other as possible and close to the strain peak. However, the amount of damping added when the active patch is centered around the strain peak is less than when the CLD is placed at the peak. This is due to limitations of the controller and actuator. If a higher control gain were used, more damping could be achieved with the PZT. Higher control gains can lead to instability of the controller, therefore this is not always desirable. Furthermore in this configuration, if the active component were to fail, the amount of damping added by the CLD is less than in the previous configuration. The damping ratio here is 0.04, this is because it is not located at the strain energy peak.

Position ($\frac{x}{L}$)	ζ	f_n
0.05	0.05	100
0.1	0.04	93.3
0.15	0.03	92.8
0.20	0.04	96.0
0.25	0.05	101
0.3	0.06	105

Table 8: Hybrid damping performance with varying CLD placement

3.3.3 Shared strain peak

Another possible configuration is one where the passive and active treatments cover the same percentage of the strain energy peak. A CLD treatment and PZT treatment of equal lengths, 15 % of the beam are selected. They are placed in the middle of the peak for the 2^{nd} eigenmode and the damping ratio is determined, with the same controller parameters as in previous runs. This configuration is illustrated in figure 11.

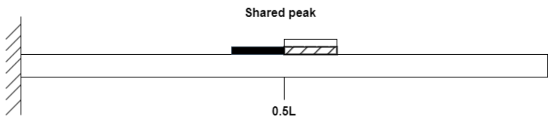

Figure 11: PZT and CLD shared strain peak

The frequency response function of this configuration is shown in figure 12. Here a damping ratio is found of 0.097. The target eigenfrequency has not shifted much, however, the first eigenfrequency has shifted by 15 % due to the controller adding flexibility to the system, as mentioned in 2.3.2. When the active control is turned off, the passive component achieves a damping ratio of 0.067, which is close to what it can achieve when placed in the middle of the strain peak. When targetting a single mode, this configuration performs better than when the PZT is centered at the peak, but still falls short in terms of damping performance when compared to CLD at the peak.

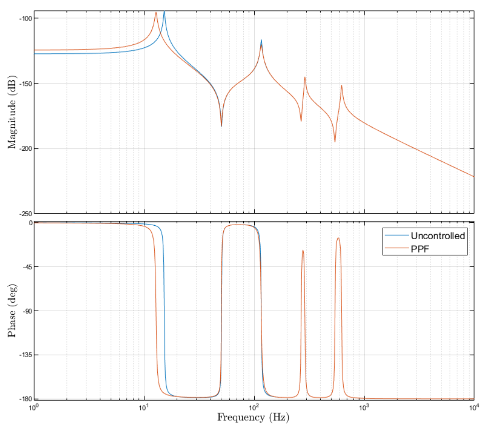

Figure 12: FRF of hybrid damping with PZT and CLD placed at strain peak

3.3.4 Hybrid vs. passive vs. active damping

It can be concluded from the previous sections that when one wishes to design a hybrid damping system, the best course of action is to place the passive treatment at the strain peak with an adjoining active treatment. These hybrid cases were compared with each other by using the same controller parameters and patch dimensions. Now the controller parameters will be tuned optimally, to compare the performance of this hybrid configuration to the either purely passive or purely active systems.

Hybrid damping

The same configuration for hybrid damping is used as in 3.3.1, this is also illustrated in figure 13 . The controller is tuned to achieve largest damping factor while satisfying stability criteria. A maximum damping ratio of 0.20 can be achieved for the second mode. This is with a damping treatment that has a total mass of 5 g.

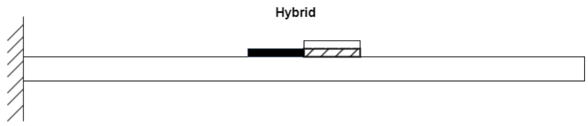

Figure 13: Beam with hybrid damping configuration for second mode

Passive damping

In comparison, to achieve similar performance for damping the second mode with passive damping, a patch covering approximately 40 % of the beam would be necessary and also weighing 5 g. It can also be observed that the dynamics of the system change significantly when only the passive method is used, the second eigenfrequency shifts up by 29 %, from 117 Hz to 151 Hz. Whereas in the case of hybrid damping, this change is only 1.2 %.

Active damping

When comparing the hybrid configuration with pure active damping, there are more factors to take into account. The amount of damping added depends not on just the size of the actuator but also on the control voltage supplied to it. If the gain of the controller is increased, a smaller patch could theoretically add as much damping as a larger one, depending on hardware limitations. To achieve a similar result as the hybrid configuration with PZT patch of the same mass, the gain of the controller is increased with a factor 15. The eigenfrequency is decreased by 3 %, which is a relatively small change. Furthermore, when only using active damping, the system is less robust. The PPF controller is sensitive to variations and if the system failed entirely, there would be no added damping to the the host structure at all.

Therefore, when damping a single mode, the hybrid method has several advantages over either purely passive or active methods. Hybrid treatments offer good performance for the same weight as passive damping, less change in system dynamics, added robustness compared to AVC, and much lower control voltages.

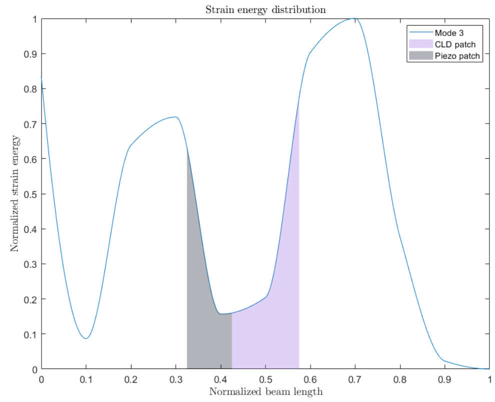

Figure 14: Strain energy distribution of 3^{rd} mode with damping treatment for 2^{nd} mode

3.4 Hybrid damping for multiple modes

When considering adding damping to a system, it is often the wish to suppress vibration across a broad frequency range. In the previous section, a single mode was targeted, in this section the aim is to achieve better damping for the first three eigenmodes. First the influence of the previous hybrid configurations on other eigenmodes are studied, then various solutions are investigated to dampen multiple modes.

3.4.1 Influence of single mode hybrid damping on other modes

The previous section has revealed that is it most desirable to have the passive treatment at the strain peak with an active patch placed next to it. This offered the most damping for a single mode as well as the added benefit of good passive damping if the active system were to fail. However, when the configuration is used as shown in figure 13, this places the CLD patch and PZT patch largely at a node of the 3^{rd} mode, see figure 14. This results in poor damping for this mode with $\zeta = 0.008$. With regards to the 1^{st} mode, viscoelastics perform worse at low frequencies and the placement is also at a location with low strain energy, therefore the amount of damping added is also small, $\zeta = 0.019$.

When the PZT is placed at the strain peak and the CLD next to it, to match the configuration of section 3.3.2, the damping performance for the targeted mode is worse than in the previous configuration. However, the damping for the other two modes has improved. The 1^{st} mode now has a damping ratio $\zeta = 0.035$ and the 3^{rd} mode has $\zeta = 0.048$.

If a purely passive treatment is used, that performs similarly to the optimal hybrid configuration (covering 40 % of the beam), the damping of the 1^{st} and 3^{rd} mode are slightly improved. For the 1^{st} mode $\zeta = 0.022$ and for the 3^{rd} mode $\zeta = 0.031$. However, due to the added stiffness, the frequency of the 2^{nd} mode increases by 27 %.

For purely active damping, the modes higher than the one being targeted are unaffected. The controller will however have an effect on the eigenfrequencies below its cut-off frequency. To dampen multiple modes, numerous damping patches are necessary with PPF controllers running in parallel. In this case, tuning the controller parameters becomes more challenging due to control spillover, especially for low frequency modes. As previously demonstrated coupling from damping the 2^{nd} mode causes the 1^{st} mode to shift [37]. Several methods exist to reduce this spillover effect, however for simplicity, the choice is made to use a single PPF controller to demonstrate the working principles of active vibration control.

3.4.2 Damping multiple modes

The previous section has demonstrated that the optimal placement for one mode, might be the worst possible for another. The most important factor in determining the amount of added damping is placing the treatment in a location of maximum strain. However, as seen for the 2^{nd} mode, its strain energy peak is at the a node of the 3^{rd} mode. Therefore a possible solution is simply to add an extra damping patch at the strain energy peak of the third mode. To reduce system complexity, the choice is made to add a second passive CLD patch, that covers 10 % of the energy peak around 0.7 times the beam length.

The results shown in 15 are indeed an improvement over the configuration from 3.3.1. Figure 15, shows the difference between an undamped beam, the hybrid beam for mode 2 and the hybrid beam with the additional CLD patch for mode 3. This is with the controller off, to purely showcase the influence of the extra passive patch. The damping ratio for the 3^{rd} mode is now 0.036, which is a large improvement over the previous configuration. Additionally, the extra patch also slightly increases the damping performance of the second mode. However, it can also be observed that the additional damping patch increases the stiffness and shifts the resonance peaks to the right.

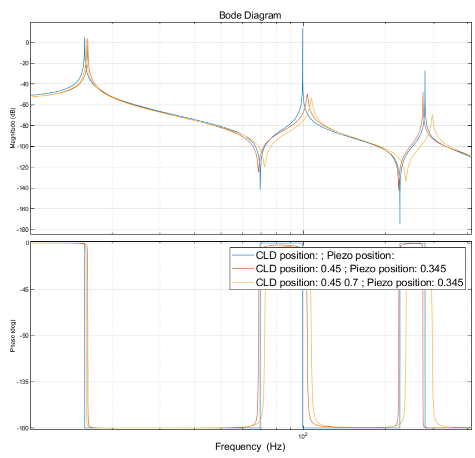

Figure 15: Undamped beam versus beam with 1 and 2 CLD patches

The first mode has remained largely unchanged by the previous additions to the system. Viscoelastic materials perform poorly at low frequencies, therefore for the first mode it is favorable to use an active damping patch for this mode. The maximum strain energy is found at the base and decreases throughout the length of the beam. The damping ratio of the first mode becomes 0.14 when a PZT patch is placed just above the base of the beam and with a controller tuned to the 1^{st} eigenfrequency. This configuration is shown in figure 16. To achieve the same performance for the 1^{st} mode using a passive patch, it would need to be twice as long as the PZT. Additional damping is required for other resonances.

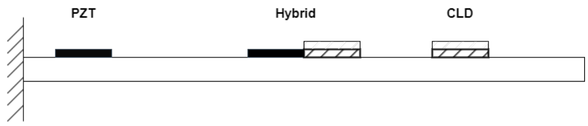

Figure 16: Hybrid damping configuration for first three modes

The same process is repeated, now with the third mode as the target frequency. A hybrid treatment is applied at its strain peak. The CLD patch is made shorter, since the strain peak at 0.7 is shorter than that of the 2^{nd} mode. The damping factor achieved for this mode with the hybrid treatment is 0.104. The 1^{st} and 2^{nd} modes however are poorly damped in this configuration. Therefore, the second mode is damped with a CLD patch, and the first mode with an active patch. The damping ratios of the first three modes are then 0.19, 0.08 and 0.14 respectively. This is an overall improvement of approximately 25 % over a beam covered only with passive treatments of the same size at the same locations. This improvement comes with a mass penalty of 2 g over the passive case. Compared to beam with PZTs of the same size, at the same location and with the same control gain, the improvement is 75 %. However, if controller gains are increased, by factor 10, the improvement of hybrid damping reduces to 30 %. The hybrid treatment is 9 g lighter than the active configuration.

3.4.3 Hybrid vs. passive vs. active damping for multiple modes

When damping multiple modes the amount of design variables increases substantially. Finding an optimal configuration and combination of different treatments is challenging, and there are multiple possible solutions to achieve the same amount of added damping. The best choice therefore depends on the requirements and constraints imposed on the system. Each damping method tends to come with its strengths and weaknesses. Passive damping is by far the simplest solution and adds a good amount of damping if well placed. However, if too much is added, the system dynamics change significantly. It also cannot dampen the first mode as well as active damping. Active damping on the other hand is much more complex to implement, is sensitive to variations and requires careful tuning and high voltages. But it can dampen low frequencies as effectively as high frequencies and can be more easily tuned to add a specific amount of damping.

The following needs to be considered when designing a hybrid damped system for multiple modes:

- The target mode should be damped with hybrid damping,
- Adding CLD shifts the eigenfrequencies up.
- Active damping lowers the eigenfrequencies below the cut-off.
- Hybrid damping uses the least amount of space on the host structure than purely passive or active treatments for equivalent or better performance.
- Pure AVC requires much higher control gains to achieve the same amount of damping as hybrid
- Low frequencies should be damped with AVC due to VEM's poor performance

4 Conclusion

This paper explores the use of side-by-side hybrid vibration control to dampen the same mode as well as multiple modes. Using a simplified model, like the Ross-Kerwin-Ungar model, can still capture the frequency dependent behavior and provide enough insight into the damping performance of the VEM. The importance of including viscoelastic frequency dependent behavior in the model is shown. Of the parameters investigated, the placement plays the most important role. Damping patches should be placed at the location of maximum strain for a given eigenmode. The length of the treatment also plays a role, however there a balance must be found between mass and stiffness added versus the amount of added damping.

The side-by-side configuration shows to perform better than both active and passive patches of the same size, for a single mode. With the added benefits of lower control voltages, added robustness compared to AVC and less change in system dynamics comapared to CLD. When combining both methods, the CLD should be placed at the strain peak with the active patch placed right next to it. This ensures that the CLD can dissipate the most energy, and the PZT can still adequately suppress vibrations. This also makes the system perform better in the case that the PZT were to fail.

Suppressing multiple modes using hybrid damping is more complex and the best solution depends on the design requirements. It can be stated that the target mode/most dominant mode should be suppressed using the hybrid method. Other modes can be suppressed using either passive or active methods. The choice depends in most cases on the requirements. If simplicity is important, passive damping is the best solution. However, if the system dynamics cannot change much or if very high levels of damping are required, active vibration control offers a good solution. Compromises need to be made and the design evaluated on a case by case level.

References

[2] E. M. Kerwin. "Damping of flexural waves by a constrained viscoelastic layer". In: *The Journal of the Acoustical Society of America* 31 (1959), pp. 952–962.

[4] Thomas Bailey and James E. Hubbard Jr. "Distributed piezoelectric-polymer active vibration control of a cantilever beam". In: *American Institute of Aeronautics and Astronomics* 8.5 (May 1985), pp. 605–611. DOI: 10.2514/3.20029.

[6] Amr M. Baz and Jeng-Jong Ro. "Vibration control of plates with active constrained-layer damping". In: *https://doi.org/10.1117/12.208908* 2445 (May 1995), pp. 393–409. DOI: 10.1117/12.208908.

[10] M. J. Lam, D. J. Inman, and W. R. Saunders. "Vibration Control through Passive Layer Damping and Active Control". In: *Journal of Intelligent Material Systems and Structures* 8.8 (1997), pp. 663–677. DOI: 10.1177/1045389X9700800804.

[13] D. J. McTavish and P. C. Hughes. "Modeling of Linear Viscoelastic Space Structures". In: *Journal of Vibration and Acoustics* 115.1 (Jan. 1993), pp. 103–110. ISSN: 1048-9002. DOI: 10.1115/1.2930302.

[14] M. A. Trindade, A. Benjeddou, and R. Ohayon. "Modeling of Frequency-Dependent Viscoelastic Materials for Active-Passive Vibration Damping". In: *Journal of Vibration and Acoustics* 122.2 (Apr. 2000), pp. 169–174. ISSN: 1048-9002. DOI: 10.1115/1.568429.

[16] George A. Lesieutre and Usik Lee. "A finite element for beams having segmented active constrained layers with frequency-dependent viscoelastics". In: *Smart Materials and Structures* 5.5 (1996), pp. 615–627. ISSN: 09641726. DOI: 10.1088/0964-1726/5/5/010.

[18] Feng-Ming Li et al. "Vibration control of beams with active constrained layer damping". In: *Smart Materials and Structures* 17.6 (Nov. 2008), p. 065036. ISSN: 0964-1726. DOI: 10.1088/0964-1726/17/6/065036. URL: https://iopscience.iop.org/article/10.1088/0964-1726/17/6/065036%20https://iopscience.iop.org/article/10.1088/0964-1726/17/6/065036/meta.

[23] Melvin Kruik. "Location optimized hybrid damping for one-dimensional flexible structures". Master Thesis. TU Delft, 2020.

[24] CMA Vasques, RAS Moreira, and J Rodrigues. "Viscoelastic Damping Technologies-Part I: Modeling and Finite Element Implementation." In: *Journal of advanced research in Mechanical Engineering* 1.2 (2010). ISSN: 1737-9318.

[25] P Shivashankar and S Gopalakrishnan. "Review on the use of piezoelectric materials for active vibration, noise, and flow control". In: *Smart Materials and Structures* 29.5 (Mar. 2020), p. 053001. ISSN: 0964-1726. DOI: 10.1088/1361-665X/AB7541. URL: https://iopscience.iop.org/article/10.1088/1361-665X/ab7541%20https://iopscience.iop.org/article/10.1088/1361-665X/ab7541/meta.

[26] William C. Van Nostrand, Gareth J. Knowles, and Daniel J. Inman. "¡title¿Finite element model for active constrained-layer damping¡/title¿". In: *Smart Structures and Materials 1994: Passive Damping* 2193.May 1994 (1994), pp. 126–137. DOI: 10.1117/12.174091.

[27] Margaretha J. Lam, William R. Saunders, and Daniel J. Inman. "Modelling active constriained-layer-damping using Golla-Hughes-McTavish approach". In: *Smart Structures and Materials 1995: Passive Damping* 2445.May 1995 (1995), pp. 86–97. DOI: 10.1117/12.208912.

[28] Robert D Cook et al. *Concepts and applications of finite element analysis*. John wiley & sons, 2007.

[29] Kerim Gokhan Aktas and Ismail Esen. *State-Space Modeling and Active Vibration Control of Smart Flexible Cantilever Beam with the Use of Finite Element Method*. 2020, pp. 6549–6556. URL: www.etasr.com.

[30] A. Preumont et al. "The damping of a truss structure with a piezoelectric transducer". In: *Computers and Structures* 86.3-5 (2008), pp. 227–239. ISSN: 00457949. DOI: 10.1016/j.compstruc.2007.01.038.

[31] Ladislav Starek. "Optimal Ppf Controller for Multimodal Vibration Suppression". In: *Engineering* 15 (3 2008), pp. 153–173.

[32] Jeffrey J Dosch, Daniel J Inman, and Ephrahim Garcia. "A self-sensing piezoelectric actuator for collocated control". In: *Journal of Intelligent material systems and Structures* 3.1 (1992), pp. 166–185.

[33] Gary T Fagan. "An experimental investigation into active damage control systems using positive position feedback for AVC". PhD thesis. Virginia Tech, 1993.

[34] Hassaan Hussain Syed. “Comparative study between positive position feedback and negative derivative feedback for vibration control of a flexible arm featuring piezoelectric actuator”. In: *International Journal of Advanced Robotic Systems* 14.4 (2017), p. 1729881417718801. DOI: 10.1177/1729881417718801. eprint: https://doi.org/10.1177/1729881417718801. URL: https://doi.org/10.1177/1729881417718801.

[35] CJ Goh and TH Lee. “Adaptive modal parameters identification for collocated position feedback vibration control”. In: *International Journal of Control* 53.3 (1991), pp. 597–617.

[36] Stefan Fenik and Ladislav Starek. “Optimal PPF controller for multimodal vibration suppression”. In: *Engineering Mechanics* 15.3 (2008), pp. 153–173.

[37] Hani I. M. Alhasni. “Adaptive Multimodal Damping of Flexible Structures”. Master Thesis. TU Delft, 2020.

[38] Electronics Notes. *Quality factor / Q factor; formulas and equations.* URL: https://www.electronics-notes.com/articles/basic_concepts/q-quality-factor/basics-tutorial-formula.php.

[39] James Karki. *Application Report Signal Conditioning Piezoelectric Sensors.* Texas Instruments, Sept. 2000.

[40] Peter J. Torvik. *The Analysis and Design of Constrained Layer Damping Treatments.* Aug. 1980. URL: https://apps.dtic.mil/sti/citations/ADA088200.

[41] NASHIF A.D ET AL. *VIBRATION DAMPING.* Wiley-Interscience, 1985.

Part III
Conclusions and recommendations

Conclusion

This thesis project set out to complete the following research goal: Develop a design methodology for side-by-side hybrid damping by considering complex viscoelastic properties and simultaneous use of active and passive methods for the same eigenmode.
To achieve this goal the objectives stated in the introduction were completed.

Improve the viscoelastic model
The previous study into side-by-side hybrid damping used a simplified model to represent viscoelastic damping behavior [23]. This model did not include the frequency dependent characteristics of the VEM. This property however, has a big influence on the prediction of the amount of damping it can provide. This thesis project still had the aim to use a model that was easy to implement, but included the complex behavior of VEM. The choice was made to implement the Ross-Kerwin-Ungar model. It calculates a complex stiffness for a CLD element which can then be implemented into a FEM model to simulate a partially covered beam. The model has some simplifications and some limitations. It cannot be applied in cases where the thickness of the VEM or constraining layer approaches the thickness of the bar, it is only valid for thin treatments.

The model is validated with an experiment where first a bare aluminium beam is subjected to a disturbance input and its frequency response measured. Then a thin CLD strip is added to the beam and the response measured. The loss factors measured in the experiment match those of the model relatively well. However, the model seems to overestimate the amount of stiffness added by the CLD treatment. In the experiment, the eigenfrequencies barely change when CLD tape is added, whereas in the model, a shift of up to 9 % is measured. This difference could be attributed to the VEM properties not being accurately extracted from the nomograph.

The main advantage of this model over the one previously used, is the inclusion of the frequency dependence. It is also much easier to implement than other methods found in literature. The difference this addition makes versus using a fixed value for the shear modulus is shown in this paper. The varying G^* will more accurately predict the loss factor than using a fixed value. Therefore it can be concluded that its inclusion is beneficial when designing a damped system with CLD.

Investigate parameter influence
The next objective that was achieved was investigating the influence of various parameters of the damping treatments on their performance. This was to get insight into the aspects that matter most when combining them together in the hybrid case. The location of the patches on the host structure was determined to be the most important factor for both passive and active treatments. This was expected from literature and confirmed with the current model. However, when combining both to dampen a single mode a compromise needs to be found, which is discussed as part of the next goal. Other parameters such as length and thickness also play an important role and need to be chosen based on the design requirements and constraints, as this influence the stiffness, mass and coverage of the host structure.

In the case of active vibration control, the controller plays an important role. The choice was made to implement a simple controller to demonstrate the working principle of AVC. The controller was tuned using rules of thumb from literature and through a parameter sweep of its gain and damping ratio values. Values were chosen that added the most damping, while ensuring that the controller remained stable. Other methods exist to find optimal controller parameters that might have yielded better results. However, for the purposes of this study, a parameter sweep was sufficient.

Study the use of damping methods individually and together when targeting the same mode
As was concluded from the previous objective, the placement of the damping patches is critical for optimal performance. For hybrid vibration control, the choice of placement is also important. Here the strain energy peak of a mode can be covered by either the active or passive treatment, or shared by both. It is found that to achieve the most amount of added damping, the CLD patch should be placed at the strain peak, with a PZT placed right next to it. This has the added benefit of ensuring the CLD will still perform optimally if the PZT were to be turned off or fail. Compared to a purely active case, where a PZT patch of the same length as the hybrid treatment is used, the control gain is lowered by a factor 15 to achieve the same performance. When comparing to a purely passive case, a CLD patch twice as long as the hybrid treatment would be required to achieve the same amount of damping. For damping a single mode the hybrid configuration seems to be the best solution.

The paper additionally looked at the effect of the hybrid treatment on other modes, and ways to dampen multiple modes. In some cases the addition of a hybrid damping treatment at an optimal location for one mode will have little benefit for other modes. Therefore for broadband vibration suppression additional damping treatments are required. Here the choice of which method is better depends on the requirements for the system. It can be stated however, that for the first mode, AVC is ususally a better choice because of VEM's poor low frequency performance.

Final conclusions
Side-by-side vibration control offers good performance with added benefits over pure active or pure passive damping. It can be a particularly valuable addition to a system where AVC is used. It adds robustness to the system and its implementation in that case is simple. A CLD patch would simply needed to be placed next to the active patches and the controller re-tuned. However, if a system is passively damped, the addition of active components might not always be desirable. It adds complexity to the system and a need for external power. The advantage would be using a smaller footprint on the host structure, having less influence of its dynamics and increased damping. These advantages need to be weighed over the cost of increased complexity.

Recommendations

The results of this work show the benefits of side-by-side hybrid vibration control, especially when a single mode is targeted. Further research is necessary to determine optimal hybrid damping configurations for broadband vibration suppression. Some recommendations are given below that would improve this work and give more insight into the practicality of this hybrid method.

1. **Study the use of multiple hybrid treatments for broadband vibration suppression**
   The current work has observed the benefits of hybrid damping for a single mode, and looked at its effects on other modes. When considering multiple resonances, additional either active or passive patches were used for simplicity. Suppressing multiple modes with

hybrid damping may be beneficial if extra damping performance is required even though this adds complexity to the system.

2. **Validate findings experimentally**
   The model used in the study was validated with an experiment. The rest of the study was carried out purely numerically, therefore it might be beneficial to observe whether the findings about hybrid damping are also true experimentally.

3. **Use of advanced control algorithms**
   This study makes use of PPF control to target a single mode. Other more advanced control methods might be used to achieved better performance by making the system more robust or being able to react to multiple resonances. These other methods may be harder to implement and tune but the added performance benefit could be an interesting prospect.

4. **Use of more advanced VEM modelling methods**
   One of the goals of this study was to improve the VEM model to include frequency dependent behavior. The choice was made to use as simple of a model as possible to implement this. Despite the RKU model offering a good approximation of the damping ratios of CLD, it is limited to the frequency domain and to cases where the CLD is much thinner than the host structure. Other more complex modelling methods such as the Gollah-Hughes-MacTavish (GHM) or Anaelastic Displacement Field (ADF) methods offer more insight into VEM behavior, such as time domain information. However, these models are much more complex to implement and increase the system size substantially, thus increasing the computational effort required.

References

[1] D.E. Adams. “Mechanical Vibrations”. In: *Purdue University* (2010), pp. 1–7. URL: `https://engineering.purdue.edu/~deadams/ME563/notes_10.pdf`.

[2] E. M. Kerwin. “Damping of flexural waves by a constrained viscoelastic layer”. In: *The Journal of the Acoustical Society of America* 31 (1959), pp. 952–962.

[3] G Barac. “Hitchhikers guide to damping”. Delft University of Technology, 2020, pp. 1–23.

[4] Thomas Bailey and James E. Hubbard Jr. “Distributed piezoelectric-polymer active vibration control of a cantilever beam”. In: *American Institute of Aeronautics and Astronomics* 8.5 (May 1985), pp. 605–611. DOI: `10.2514/3.20029`.

[5] B Azvine, G R Tomlinson, and R J Wynne. “Use of active constrained-layer damping for controlling resonant vibration”. In: *Smart Materials and Structures* 4.1 (Mar. 1995), p. 1. ISSN: 0964-1726. DOI: `10.1088/0964-1726/4/1/001`.

[6] Amr M. Baz and Jeng-Jong Ro. “Vibration control of plates with active constrained-layer damping”. In: *https://doi.org/10.1117/12.208908* 2445 (May 1995), pp. 393–409. DOI: `10.1117/12.208908`.

[7] S C Huang, D J Inman, and E M Austin. “Some design considerations for active and passive constrained layer damping treatments”. In: *Smart Materials and Structures* 5.3 (June 1996), p. 301. ISSN: 0964-1726. DOI: `10.1088/0964-1726/5/3/008`.

[8] A. Benjeddou. “Advances in Hybrid Active-Passive Vibration and Noise Control Via Piezoelectric and Viscoelastic Constrained Layer Treatments:” in: *Journal of Vibration and Control* 7.4 (Aug. 2000), pp. 565–602. DOI: `10.1177/107754630100700406`.

[9] Marcelo A Trindade and Ayech Benjeddou. “Hybrid Active-Passive Damping Treatments Using Viscoelastic and Piezoelectric Materials: Review and Assessment”. In: *Journal of Vibration Control* 8 (2002), pp. 699–745. DOI: `10.1177/1077546029186`.

[10] M. J. Lam, D. J. Inman, and W. R. Saunders. “Vibration Control through Passive Layer Damping and Active Control”. In: *Journal of Intelligent Material Systems and Structures* 8.8 (1997), pp. 663–677. DOI: `10.1177/1045389X9700800804`.

[11] Joseph Plattenburg, Jason T. Dreyer, and Rajendra Singh. “Active and passive damping patches on a thin rectangular plate: A refined analytical model with experimental validation”. In: *Journal of Sound and Vibration* 353 (Sept. 2015), pp. 75–95. ISSN: 0022-460X. DOI: `10.1016/J.JSV.2015.05.026`.

[12] R Stanway, J A Rongong, and N D Sims. “Active constrained-layer damping: A state-of-the-art review:” in: *Journal of Systems and Control Engineering* 217.6 (Aug. 2003), pp. 437–456. DOI: `10.1177/095965180321700601`.

[13] D. J. McTavish and P. C. Hughes. “Modeling of Linear Viscoelastic Space Structures”. In: *Journal of Vibration and Acoustics* 115.1 (Jan. 1993), pp. 103–110. ISSN: 1048-9002. DOI: `10.1115/1.2930302`.

[14] M. A. Trindade, A. Benjeddou, and R. Ohayon. “Modeling of Frequency-Dependent Viscoelastic Materials for Active-Passive Vibration Damping”. In: *Journal of Vibration and Acoustics* 122.2 (Apr. 2000), pp. 169–174. ISSN: 1048-9002. DOI: `10.1115/1.568429`.

[15] R. Moreira and J. D. Rodrigues. “Constrained Damping Layer Treatments: Finite Element Modeling:” in: *Journal of Vibration and Control* 10.4 (Aug. 2003), pp. 575–595. DOI: `10.1177/1077546304039060`.

[16] George A. Lesieutre and Usik Lee. “A finite element for beams having segmented active constrained layers with frequency-dependent viscoelastics”. In: *Smart Materials and Structures* 5.5 (1996), pp. 615–627. ISSN: 09641726. DOI: `10.1088/0964-1726/5/5/010`.

[17] J. B. Kosmatka and S. L. Liguore. "Review of Methods for Analyzing ConstrainedLayer Damped Structures". In: *Journal of Aerospace Engineering* 6.3 (July 1993), pp. 268–283. DOI: `10.1061/(ASCE)0893-1321(1993)6:3(268)`.

[18] Feng-Ming Li et al. "Vibration control of beams with active constrained layer damping". In: *Smart Materials and Structures* 17.6 (Nov. 2008), p. 065036. ISSN: 0964-1726. DOI: `10.1088/0964-1726/17/6/065036`. URL: `https://iopscience.iop.org/article/10.1088/0964-1726/17/6/065036%20https://iopscience.iop.org/article/10.1088/0964-1726/17/6/065036/meta`.

[19] Vivek Gupta, Manu Sharma, and Nagesh Thakur. "Optimization Criteria for Optimal Placement of Piezoelectric Sensors and Actuators on a Smart Structure: A Technical Review:" in: *Journal of Intelligent Material Systems and Structures* 21.12 (Sept. 2010), pp. 1227–1243. DOI: `10.1177/1045389X10381659`. URL: `https://journals.sagepub.com/doi/abs/10.1177/1045389x10381659`.

[20] P. Aumjaud et al. "Multi-objective optimisation of viscoelastic damping inserts in honeycomb sandwich structures". In: *Composite Structures* 132 (Nov. 2015), pp. 451–463. ISSN: 0263-8223. DOI: `10.1016/J.COMPSTRUCT.2015.05.061`.

[21] Yi Cheng Chen and Shyh Chin Huang. "An optimal placement of CLD treatment for vibration suppression of plates". In: *International Journal of Mechanical Sciences* 44.8 (Aug. 2002), pp. 1801–1821. ISSN: 0020-7403. DOI: `10.1016/S0020-7403(02)00042-5`.

[22] J. Ducarne, O. Thomas, and J. F. Deü. "Placement and dimension optimization of shunted piezoelectric patches for vibration reduction". In: *Journal of Sound and Vibration* 331.14 (July 2012), pp. 3286–3303. ISSN: 0022-460X. DOI: `10.1016/J.JSV.2012.03.002`.

[23] Melvin Kruik. "Location optimized hybrid damping for one-dimensional flexible structures". Master Thesis. TU Delft, 2020.

[24] CMA Vasques, RAS Moreira, and J Rodrigues. "Viscoelastic Damping Technologies-Part I: Modeling and Finite Element Implementation." In: *Journal of advanced research in Mechanical Engineering* 1.2 (2010). ISSN: 1737-9318.

[25] P Shivashankar and S Gopalakrishnan. "Review on the use of piezoelectric materials for active vibration, noise, and flow control". In: *Smart Materials and Structures* 29.5 (Mar. 2020), p. 053001. ISSN: 0964-1726. DOI: `10.1088/1361-665X/AB7541`. URL: `https://iopscience.iop.org/article/10.1088/1361-665X/ab7541%20https://iopscience.iop.org/article/10.1088/1361-665X/ab7541/meta`.

[26] William C. Van Nostrand, Gareth J. Knowles, and Daniel J. Inman. "¡title¿Finite element model for active constrained-layer damping¡/title¿". In: *Smart Structures and Materials 1994: Passive Damping* 2193.May 1994 (1994), pp. 126–137. DOI: `10.1117/12.174091`.

[27] Margaretha J. Lam, William R. Saunders, and Daniel J. Inman. "Modelling active constrianed-layer-damping using Golla-Hughes-McTavish approach". In: *Smart Structures and Materials 1995: Passive Damping* 2445.May 1995 (1995), pp. 86–97. DOI: `10.1117/12.208912`.

[28] Robert D Cook et al. *Concepts and applications of finite element analysis.* John wiley & sons, 2007.

[29] Kerim Gokhan Aktas and Ismail Esen. *State-Space Modeling and Active Vibration Control of Smart Flexible Cantilever Beam with the Use of Finite Element Method.* 2020, pp. 6549–6556. URL: `www.etasr.com`.

[30] A. Preumont et al. "The damping of a truss structure with a piezoelectric transducer". In: *Computers and Structures* 86.3-5 (2008), pp. 227–239. ISSN: 00457949. DOI: `10.1016/j.compstruc.2007.01.038`.

[31] Ladislav Starek. “Optimal Ppf Controller for Multimodal Vibration Suppression”. In: *Engineering* 15 (3 2008), pp. 153–173.

[32] Jeffrey J Dosch, Daniel J Inman, and Ephrahim Garcia. “A self-sensing piezoelectric actuator for collocated control”. In: *Journal of Intelligent material systems and Structures* 3.1 (1992), pp. 166–185.

[33] Gary T Fagan. “An experimental investigation into active damage control systems using positive position feedback for AVC”. PhD thesis. Virginia Tech, 1993.

[34] Hassaan Hussain Syed. “Comparative study between positive position feedback and negative derivative feedback for vibration control of a flexible arm featuring piezoelectric actuator”. In: *International Journal of Advanced Robotic Systems* 14.4 (2017), p. 1729881417718801. DOI: 10.1177/1729881417718801. eprint: https://doi.org/10.1177/1729881417718801. URL: https://doi.org/10.1177/1729881417718801.

[35] CJ Goh and TH Lee. “Adaptive modal parameters identification for collocated position feedback vibration control”. In: *International Journal of Control* 53.3 (1991), pp. 597–617.

[36] Stefan Fenik and Ladislav Starek. “Optimal PPF controller for multimodal vibration suppression”. In: *Engineering Mechanics* 15.3 (2008), pp. 153–173.

[37] Hani I. M. Alhasni. “Adaptive Multimodal Damping of Flexible Structures”. Master Thesis. TU Delft, 2020.

[38] Electronics Notes. *Quality factor / Q factor; formulas and equations.* URL: https://www.electronics-notes.com/articles/basic_concepts/q-quality-factor/basics-tutorial-formula.php.

[39] James Karki. *Application Report Signal Conditioning Piezoelectric Sensors.* Texas Instruments, Sept. 2000.

[40] Peter J. Torvik. *The Analysis and Design of Constrained Layer Damping Treatments.* Aug. 1980. URL: https://apps.dtic.mil/sti/citations/ADA088200.

[41] NASHIF A.D ET AL. *VIBRATION DAMPING.* Wiley-Interscience, 1985.

[42] 3M. *3M™ Viscoelastic Damping Polymer 112 Series, Technical Data.* Retrieved from https://multimedia.3m.com/mws/media/8281340/3m-viscoelastic-damping-polymer-112-series.pdf?fn=Viscoelastic. 2015.

[43] PI Ceramic. *DuraAct Patch Transducer.* Retrieved from https://static.piceramic.com/fileadmin/user_upload/physik_instrumente/files/datasheets/P-876-Datasheet.pdf?_gl=1*1fiuul8*_ga*OTQ4MTUxMTk0LjE2NjAzMDUzMjc.*_ga_5LE7T6QFKF*MTY2MTgzOTMyOC4zLjAuMTY2MTgzOTMyOC4wLjAuMA... 2020.

[44] PiezoDrive. *BD-300 V5 Datasheet.* Retrieved from https://www.piezodrive.com/wp-content/uploads/2021/01/BD300-V5-Datasheet-R6.pdf. 2021.

[45] J. Karki. *Signal Conditioning Piezoelectric Sensors.* Retrieved from https://www.ti.com/lit/an/sloa033a/sloa033a.pdf. 2000.

Appendices

A Finite element model

A.1 Euler-Bernoulli beam model

The model used to simulate the beam uses one dimensional Euler-Bernoulli beam elements for the host structure. The governing equations of motion for the beam for forced motion can be written as a fourth order partial differential equation [29]:

$$\rho A \frac{\partial^2 v(x,t)}{\partial t^2} + EI \frac{\partial^4 v(x,t)}{\partial x^4} = F_{ext}, \tag{A.1}$$

where v is the displacement of the beam, ρ the density, A the cross-sectional area, E the Young's Modulus, I the moment of inertia and F_{ext} the external force. To obtain the shape functions we can assume the displacement v to be a cubic polynomial:

$$v(x,t) = a_1 x^3 + a_2 x^2 + a_3 x + a_4, \tag{A.2}$$

where, a_i indicates the total degree of freedom including displacement and rotation for each element. These constants are obtained with appropriate boundary conditions. The displacement can be written in the form:

$$v(x,t) = \begin{bmatrix} N_1(x) & N_2(x) & N_3(x) & N_4(x) \end{bmatrix} \begin{bmatrix} v_1 \\ \theta_1 \\ v_2 \\ \theta_2 \end{bmatrix} = [N][u] \tag{A.3}$$

Here $[N]$ represents the shape functions and $[u]$ the nodal displacement vector. Since the beam is considered clamped at one end the first two degrees of freedom are set to zero $v_1 = \theta_1 = 0$. The bending moment is calculated as follows:

$$M = EI \frac{\partial^2 u}{\partial x^2}, \tag{A.4}$$

with the bending moment the potential and kinetic energy of the beam can be found with:

$$U = \frac{EI}{2} \int_0^L (\frac{\partial^2 v}{\partial x^2})^2 dx = \frac{EI}{2} \int_0^L [u]^T [N_{xx}]^T [N_{xx}][u] dx = \frac{1}{2}[u]^T (EI \int_0^L [N_{xx}]^T [N_{xx}] dx)[u], \tag{A.5}$$

$$T = \frac{\rho A}{2} \int_0^L (\frac{\partial v}{\partial t})^2 dt = \frac{\rho A}{2} \int_0^L [\dot{u}]^T [N_t]^T [N_t][\dot{u}] dt = \frac{1}{2}[\dot{u}](\rho A \int_0^L [N_t]^T [N_t] dt)[\dot{u}]. \tag{A.6}$$

Here N_{xx} represents the second spatial derivative of the shape function, N_t represents the time derivative of the space function. These energies can also be expressed as follows:

$$U = \frac{1}{2}[u]^T [K_e][u], \tag{A.7}$$

$$T = \frac{1}{2}[\dot{u}]^T [M_e][\dot{u}], \tag{A.8}$$

where K_e and M_e represent the stiffness and mass matrices respectively. These have are expressed as follows:

$$K_e = \frac{EI}{L^3} \begin{bmatrix} 12 & 6L & -12 & 6L \\ 6L & 4L^2 & -6L & 2L^2 \\ -12 & -6L & 12 & -6L \\ 6L & 2L^2 & -6L & 4L^2 \end{bmatrix}, \tag{A.9}$$

$$M_e = \frac{\rho A L}{420}\begin{bmatrix} 156 & 22L & 54 & -13L \\ 22L & 4L^2 & 13L & -3L^2 \\ 54 & 13L & 156 & -22L \\ -13L & -3L^2 & -22L & 4L^2 \end{bmatrix} \tag{A.10}$$

A.2 Piezoelectric model

The piezoelectric patch element can be modelled using the same approach as for the Euler Bernoulli beam element [29]. The mass and stiffness matrices are expressed as follows:

$$K_p = \frac{E_p I_p}{L^3}\begin{bmatrix} 12 & 6L & -12 & 6L \\ 6L & 4L^2 & -6L & 2L^2 \\ -12 & -6L & 12 & -6L \\ 6L & 2L^2 & -6L & 4L^2 \end{bmatrix}, \tag{A.11}$$

$$M_p = \frac{\rho_p A_p L}{420}\begin{bmatrix} 156 & 22L & 54 & -13L \\ 22L & 4L^2 & 13L & -3L^2 \\ 54 & 13L & 156 & -22L \\ -13L & -3L^2 & -22L & 4L^2 \end{bmatrix}, \tag{A.12}$$

with the subscript p denoting a piezoelectric property. However, since the piezoelectric patches are bonded to the beam in a collocated configuration, the stiffness of the whole element including the host structure is expressed by:

$$EI_{eq} = EI + 2E_p I_p, \tag{A.13}$$

and I_p is calculated with the parallel axis theorem:

$$I_p = \frac{1}{12} w h_p^3 + w h_p \frac{(h_b + h_p)^2}{4}, \tag{A.14}$$

where h_p and h_b being the height of the piezoelectric patch and beam respectively. The mass per unit length is:

$$(\rho A)_{eq} = w(\rho h_b + 2\rho_p h_p). \tag{A.15}$$

Then the stiffness and mass matrices of these elements can be expressed as follows:

$$K_{ep} = \frac{EI_{eq}}{L^3}\begin{bmatrix} 12 & 6L & -12 & 6L \\ 6L & 4L^2 & -6L & 2L^2 \\ -12 & -6L & 12 & -6L \\ 6L & 2L^2 & -6L & 4L^2 \end{bmatrix}, \tag{A.16}$$

$$M_{ep} = \frac{(\rho A)_{eq} L}{420}\begin{bmatrix} 156 & 22L & 54 & -13L \\ 22L & 4L^2 & 13L & -3L^2 \\ 54 & 13L & 156 & -22L \\ -13L & -3L^2 & -22L & 4L^2 \end{bmatrix}. \tag{A.17}$$

A.3 Viscoelastic model

The constrained layer damping element containing a viscoelastic core is modelled using the Ross-Kerwin-Ungar model. This model depicts a three layer sandwich beam, seen in figure 17. From the RKU model, one can obtain a complex stiffness for the CLD element that depicts its frequency dependent behavior. The model uses the complex Young's Modulus and complex shear modulus that can be obtained from experimental data. This data can then be interpolated over a desired frequency range.

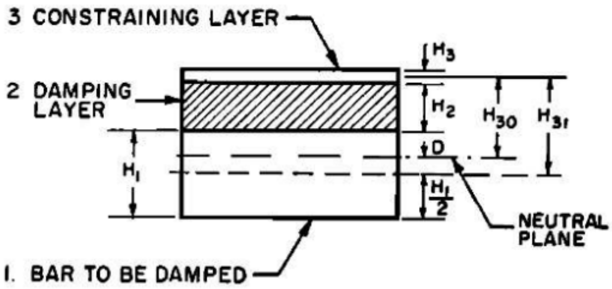

Figure 17: Section of a CLD elementv [2]

The complex moduli can be written as follows:

$$G^*(j\omega) = G^{'}(\omega)[1 + j\eta(\omega)], \tag{A.18}$$

$$E^*(j\omega) = 2(1 + \nu_v)G^{'}(j\omega). \tag{A.19}$$

The RKU model expresses the bending stiffness of the CLD element with a complex value. This value changes with the frequency that the beam is excited at, because it depends on G^* and E^*. This bending stiffness can be included in the FEM model to simulate a partially covered beam. The bending stiffness is expressed as:

$$\begin{aligned} EI^* = E_1(\frac{H_1^3}{12} + H_1D^2) + E_2^*(\frac{H_2^3}{12}H + H_2(H_{21} - D^2)) + E_3(\frac{H_3^3}{12} + H_3(H_{31} - D^2)) - \\ E_2^*\frac{H_2^2}{12}(\frac{H_{31} - D}{1+g}) - [\frac{E_2^*H_2}{2}(H_{21} - D) + E_3H_3(H_{31} - D)](\frac{H_{31} - D}{1+g}). \end{aligned} \tag{A.20}$$

The complex stiffness contains the following parameters:

$$D = \frac{E_2^*H_2(H_{31} - \frac{H_{21}}{2})g(E_2^*H_2H_{21} + E_3H_3H_{31})}{E_1H_1 + \frac{E_2^*H_2}{2}g(E_1H_1 + E_2^*H_2 + E_3H_3)}, \tag{A.21}$$

$$g = \frac{G_2^*}{E_3H_2H_3p^2}, \tag{A.22}$$

$$H_{21} = \frac{H_1 + H_2}{2}, \tag{A.23}$$

$$H_{31} = \frac{H_1 + H_3}{2} + H_2. \tag{A.24}$$

The bending stiffness is then included into the stiffness matrix for the CLD element:

$$K_v = \frac{EI^*}{L^3}\begin{bmatrix} 12 & 6L & -12 & 6L \\ 6L & 4L^2 & -6L & 2L^2 \\ -12 & -6L & 12 & -6L \\ 6L & 2L^2 & -6L & 4L^2 \end{bmatrix}. \tag{A.25}$$

The mass matrix is similar to the previously derived ones, with the mass per unit length being substituted with the mass of base beam, mass of VEM layer and mass of constraining layer.

A.4 System matrix assembly

To assemble the system mass and stiffness matrices the beam is divided up into different elements. Either bare beam, piezoelectric or CLD. For each element the relevant stiffness and mass matrices are assembled. These are then combined in the appropriate order in which they appear along the beam in the system matrices. Kruik [23] has provided an example for a 2 element system. The element stiffness matrix has entries K^i_{node} which represents the i^{th} node DoFs, which is part of the $K^i_{element}$.

$$K^i_{element} = \begin{bmatrix} K^{2i-1}_{node} & 0 \\ 0 & K^{2i}_{node} \end{bmatrix} \tag{A.26}$$

$$K_{system} = \begin{bmatrix} 1 & 0 & 0 & 0 \\ 0 & 1 & 1 & 0 \\ 0 & 0 & 0 & 1 \end{bmatrix} \begin{bmatrix} K^1_{node} & 0 & 0 & 0 \\ 0 & K^2_{node} & 0 & 0 \\ 0 & 0 & K^3_{node} & \\ 0 & 0 & 0 & K^4_{node} \end{bmatrix} \begin{bmatrix} 1 & 0 & 0 \\ 0 & 1 & 0 \\ 0 & 1 & 0 \\ 0 & 0 & 1 \end{bmatrix} \tag{A.27}$$

A.5 Frequency response

The stiffness matrix becomes complex and changes with frequency. Therefore the equations of motion are transformed into the frequency domain. For the FEM model the following equation of motion is obtained:

$$[-\omega^2\mathbf{M} + \mathbf{K}(j\omega)]\mathbf{U}(j\omega) = \mathbf{F}(j\omega) \tag{A.28}$$

The matrices $\mathbf{K}$ and $\mathbf{M}$ are made up of the beam elements, piezoelectric elements and the CLD elements. As is implied in the formula, K is dependent on ω. To solve this equation and to generate frequency response plots, this equation is solved for the displacements U at each frequency of interest. In this case 10 000 points are selected between 1 and 1000 Hz. Then a bode diagram can be generated with the displacement of the node of interest as an output and the disturbance force as an input. This process is described in figure 18

Figure 18: Process to calculate frequency response of system

$\mathbf{K}^E$ represents the elastic part of the stiffness matrix, $\mathbf{K}^V$ the viscoelastic and frequency dependent part. H_{oi} is the transfer function from the o^{th} node where the external force is applied to the i^{th} node where the strain is measured. Using this transfer function, Bode diagrams of the system can be generated.

B Experimental validation

B.1 Host structure

The model used is tested and validated with an experiment. An existing setup created by a previous TU Delft student [37] was used, with some slight modifications for this thesis. An aluminium cantilver beam is the host structure for this experiment. It is clamped at its base and oriented vertically. The properties of the beam are give in table 1.

B.2 Constrained layer damping treatment

A constrained layer damping tape is used to apply damping to the beam. 3M 2552 Damping Foil was applied onto the beam. This CLD tape is used to dampen resonant vibrations across a wide range of frequencies and temperatures. It is constructed of an aluminium constraining layer and pressure sensitive viscoelastic polymer adhesive. The viscoelastic layer is 0.127 mm thick and the constraining layer is twice as thick at 0.254 mm. The viscoelastic properties are extracted from the nomograph below.

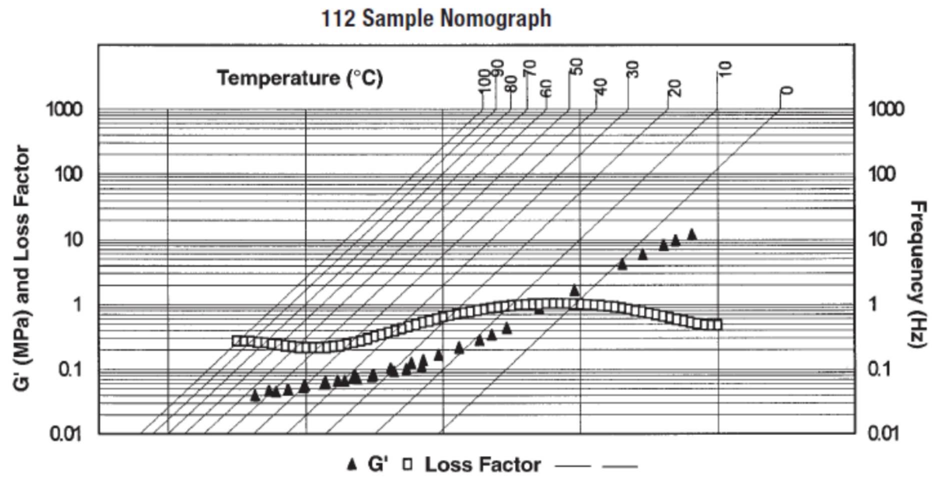

Figure 19: Nomograph CLD damping tape [42]

This is done by selecting a frequency line, then following that line where it intersects an isotherm line. Then a vertical line is extended between this intersection point to the loss factor and shear modulus. The following values were extracted from the graph. Then interpolation is performed using MATLAB piecewise cubic Hermite interpolating polynomial, using 10 000 points accross the frequency range.

Frequency f	1	10	100	1000
Shear modulus G' (MPa)	0.2	0.8	1.2	8
Loss factor η	0.7	1	0.9	0.5

Table 9: Shear modulus and loss factor extracted from nomograph

A 10 cm long and 3.5 cm wide piece of CLD tape is placed on the beam, just above the piezoelectric transducers, 8 cm from the base. This was an arbitrary location, the experiment was performed only to check the validity of the model and not to check an optimal configuration.

B.3 Piezoelectric transducers

The piezoelectric transducers used in this experiment are PI Ceramic P-876.A12 DuraAct patch transducers, the properties can be found in table 10. Two of these transducers are placed on opposite sides of the beam, acting as a collocated sensor-actuator pair. The pair is placed 1 cm above the base of the beam. The patches are attached to the beam using epoxy glue. The patches have voltage connections that can be soldered onto. These patches are connected to two different amplifier circuits. The actuator is connected to a voltage amplifier circuit and the sensor to a charge amplifier circuit.

Property	Value	Unit
Operating voltage range	-100 to 400	V
Motion and positioning		
Min lateral contraction	650	μm/m
Rel. lateral contraction	1.3	μm/m/V
Mechanical properties		
Blocking force	90	N
Min. bending radius	20	mm
Drive properties		
Electrical capacitance	90	nF
Piezo ceramic	PIC255	
Piezoceramic height	200	μm
Miscellaneous		
Voltage connector	Soldering points	
Dimensions	61 x 35 x 0.5	mm

Table 10: PI-876.A12 properties [43]

The voltage amplifier circuit uses a PiezoDrive BD-300 amplifier. This is used to achieve the high voltages required to drive the actuator. The input signal comes from a micro-controller and ranges between 0 and 3 V. This signal can then be amplified to $\pm$ 300 V thanks to the amplifier. In this case the signal is amplified to approximately 30 V. The properties and wiring diagram are provided below.

Property	Value	Unit
Supply Voltage	12-30	V
Input voltage range	0-3	V
Input impedance	5-10	
Output voltage	300	V
Differential output	$\pm$ 300	V
Gain	101	
Peak current	50	mA
RMS current	11	mA
Small signal bandwidth	20	kHz

Table 11: BD-300 amplifier properties [37]

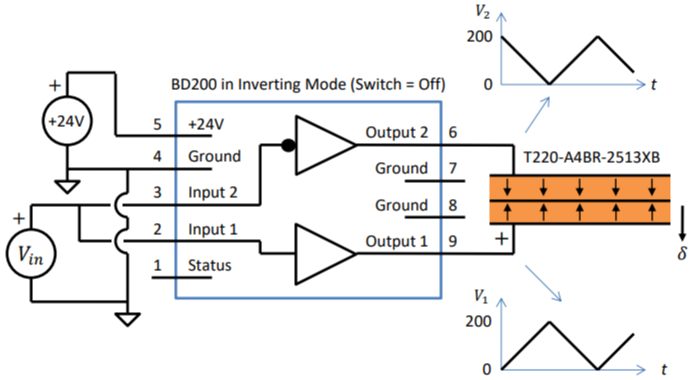

Figure 20: Voltage amplifier wiring diagram [44]

The charge amplifier circuit used with the sensor conditions the signal, it produces a suitable voltage output proportional to the charge of the sensor by intergrating the generated current. It has further advantages such as improving low frequency measurements, negating possible disturbances due to capacitors parallel to the sensor and preventing measurement drift [37]. The circuit diagram is provided and is based on an operational amplifier (OP497). A feedback capacitor C_f is used for integration, a feeback resistor R_f provides a discharge path to prevent saturation and the input resistor R_i protects against electrostatic discharge.

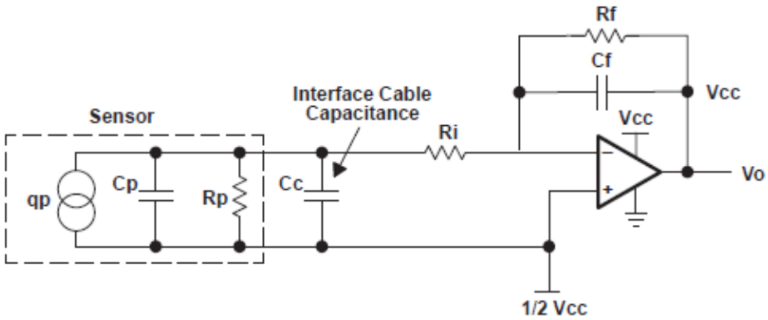

Figure 21: Circuit diagram for charge amplifier circuit [45]

B.4 System Identification

The Texas Instruments C2000 Delfino MCU F28379D LaunchPad™ is used to send and receive signals to and from the piezoelectric transducer patches. Code from Hani [37] is generated in MATLAB Simulink to send a chirp signal to the actuator. The sensor signal can be logged in the MATLAB workspace. A detailed overview of how this is done is provided in [37].

Two identifaction runs are performed to validate the model. The first is on a beam with only the collocated sensor-actuator pair and the second one with the CLD strip. The strain measurements from the sensor patch are logged and using MATLAB $tfestimate$ Bode plots are generated, see figure 22. The results from this identification run are then compared with the results from the model, these are shown and discussed in section 2.4.

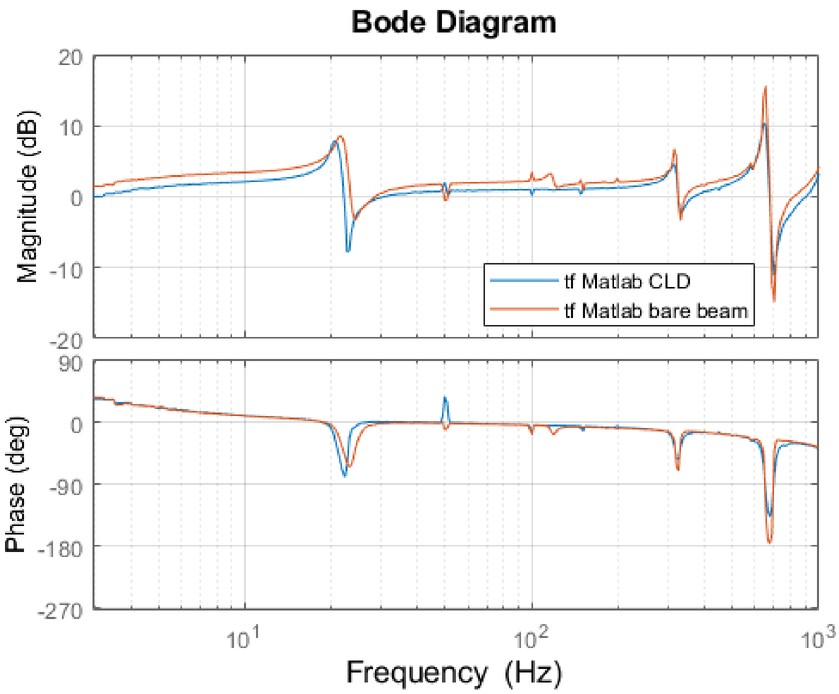

Figure 22: System identification

C MATLAB code

C.1 FEM model

```matlab
function [mf, sys, sys_fb, U, modes_index, nElem, H_oi,lossfac, en_tot, en_cld, en_bb] = batchbeam(beam,visc,cl,piez,ms,CLDpos,piezopos)

%This function calculates the state space system of a 1D Euler Bernoulli
%beam with active piezo and passive CLD elements. This code can be used to
%run batch simulations with the active and passive patches at different
%points along the beam
%Function returns mf --> uncontrolled beam and sys --> state space model w/
%control
%% First calculate visco properties
%Properties extracted from 3M ISD112 nomograph

if ms.constG == false

    nom.omega = [0.1 1 10 100 1000]; %frequency vector [Hz]
    nom.Gprime = 1e6*[0.1 0.2 0.8 1.2 8]; %shear modulus vector for discrete frequency values [Pa]
    nom.eta = [0.4 0.7 1 0.9 0.5]; %loss factor vector for discrete frequencies [Pa]
    nom.logomega = logspace(-1,3,10000); %logarithmic frequency vector for interpolation
    Gprime = pchip(nom.omega, nom.Gprime, nom.logomega);
    Eta = pchip(nom.omega, nom.eta, nom.logomega);
    G_pp = Gprime.*Eta;
    G_star = Gprime.*(1i*Eta) + Gprime ; %formula for complex shear modulus

else
    nom.omega = [0.1 1 10 100 1000]; %frequency vector [Hz]
    nom.Gprime = 1e6*[0.1 0.2 0.8 1.2 8]; %shear modulus vector for discrete frequency values [Pa]
    nom.eta = [0.4 0.7 1 0.9 0.5]; %loss factor vector for discrete frequencies [Pa]
    nom.logomega = logspace(-1,3,10000); %logarithmic frequency vector for interpolation
    Gprime = ones(1,10000)*nom.Gprime(3);
    Eta = ones(1,10000)*nom.eta(3);
    G_pp = Gprime.*Eta;
    G_star = Gprime.*(1i*Eta) + Gprime ; %formula for complex shear modulus
end
%% Lengths of different elements
```

```
n_cld = length(CLDpos); %number of cld patches
n_piezo = length(piezopos); %number of piezo patches
npatch = n_cld + n_piezo; % total number of patches
visco = zeros(1,npatch); %location of CLD patch x/L, includes
    piezo patch as well
pie = zeros(1,npatch); %location of piezo patch x/L, includes
    visco patch as well
totloc = sort([CLDpos piezopos]); %location of all patches x/L
    sorted by order in which they appear
patchlengths = zeros(1,npatch); %vector with lengths of patches
    in order of which they appear on beam

for i = 1:npatch
    if  ismember(totloc(i),piezopos) == 1 %check whether patch is
         piezo or not
    pie(i) = totloc(i); %fill in the location of piezo patch
    elseif ismember(totloc(i),CLDpos) == 1 %check whether patch
        is visco or not
        visco(i) = totloc(i); %fill in location of viscopatch
    end
end


for i = 1:npatch
  if isempty(piezopos) == 1 && isempty(CLDpos) == 1
      ms.patchlengths = [];
  else
   if i == 1 %for the first patch
    if (pie(i) == 0) && (visco(i) == 0) && (piezopos(i) == 0) %
       this is to include the possibility of patch starting at x
       =0
        patchlengths(i) = piez.L; %if the piezo patch is at x = 0
            fill in its length in the vector
    elseif (pie(i) == 0) && (visco(i) == 0) && (CLDpos(i) == 0) %
       if the CLD patch is at x = 0
        patchlengths(i) = visc.L;
    elseif pie(i) == 0 && visco(i) ~= 0 %case when the first
       patch is not at x=0 and it is a visco patch
        patchlengths(i) = visc.L;
    else visco(i) == 0 && pie(i) ~=0 %case when first patch is
       not at x =0 and is a piezo patch
        patchlengths(i) = piez.L;
    end
   else
       if pie(i) == 0
           patchlengths(i) = visc.L;
       elseif visco(i) == 0
           patchlengths(i) = piez.L;
       end
   end
```

```
  end
end


[Ls, sElements, vElements] = getLength(beam, ms, piez, visc,
   CLDpos, piezopos, visco, pie, patchlengths);
nElem = length(Ls);
nNodes = nElem +1 ;

%% Generate and assemble system matrices

K_sys = zeros(ms.nDofs*nNodes,ms.nDofs*nNodes); %set up system
   stiffness matrix
M_sys = zeros(ms.nDofs*nNodes,ms.nDofs*nNodes); %set up system
   mass matrix

F = zeros(length(K_sys),length(nom.logomega)); %set up load
   vector

if ms.tipforce == true
  F(end-1,:) = 1; %apply vertical load to last node

elseif ms.patchinput == true
    F(4,:) = 1; %simulate a patch by applying a bending moment at
        the ends of the patch
    F(6,:) = 1;
    F(8,:) = 1;
else
  F(3,:) = 1; %apply force near base of structure at first non
     clamped node
end
U = zeros(length(K_sys), length(nom.logomega)); %matrix to store
   displacements
H_oi = zeros(1,length(U));
Ph = zeros(size(H_oi));
p = 8*pi/beam.L;

for i = 1:length(nom.logomega)

    w = nom.logomega(i)*2*pi; %current frequency
    [EI_CLD, eta] = rku(beam, visc, cl, p, G_star(i), Gprime(i),
       G_pp(i)); %get RKU bending stiffness at current frequency

    for k = 1:nElem
    n1 = k; %starting node
    n2 = k+1; %end node

    [K_bb, M_bb, K_CLD, M_CLD, K_p, M_p] = ElemMat(beam,visc,cl,
       piez, Ls(k), EI_CLD); %get all the elememtal matrices


```

```
    if vElements(k) == 1 %check whether element is CLD
        Kelem = K_CLD; %elastic stiffness matrix for CLD element
        Melem = M_CLD; %mass matrix for CLD element

    elseif sElements(k) == 1 %check whether element is piezo
        Kelem = K_p; %stiffness matrix for piezo
        Melem = M_p; %mass matrix for piezo element

    else
        Kelem = K_bb; %elastic stiffness matrix for base beam
        Melem = M_bb; %mass matrix for base beam

    end

    if n1 == 1  %apply clamped boundary condition to first node
        Kelem(1:ms.nDofs,:) = zeros(ms.nDofs,ms.nDofs*2);
        Kelem(:,1:ms.nDofs) = zeros(ms.nDofs*2,ms.nDofs);
        Kelem(1:ms.nDofs,1:ms.nDofs) = eye(ms.nDofs);
        Melem(1:ms.nDofs,:) = zeros(ms.nDofs,ms.nDofs*2);
        Melem(:,1:ms.nDofs) = zeros(ms.nDofs*2,ms.nDofs);
        Melem(1:ms.nDofs,1:ms.nDofs) = eye(ms.nDofs);

    end
    K_sys(n1*ms.nDofs-(ms.nDofs-1):n2*ms.nDofs,n1*ms.nDofs-(ms.
       nDofs-1):n2*ms.nDofs) = K_sys(n1*ms.nDofs-(ms.nDofs-1):n2*
       ms.nDofs,n1*ms.nDofs-(ms.nDofs-1):n2*ms.nDofs)+ Kelem;
    M_sys(n1*ms.nDofs-(ms.nDofs-1):n2*ms.nDofs,n1*ms.nDofs-(ms.
       nDofs-1):n2*ms.nDofs) = M_sys(n1*ms.nDofs-(ms.nDofs-1):n2*
       ms.nDofs,n1*ms.nDofs-(ms.nDofs-1):n2*ms.nDofs)+ Melem;

    end


    U(:,i) = (K_sys - (w^2)*M_sys)\F(:,i);
    if ms.tipforce == true
        H_oi(:,i) = U(end-1,i)/F(end-1,i);
    elseif ms.patchinput == true
        H_oi(:,i) = U(4,i)/F(4,i);
    else
        H_oi(:,i) = U(3,i)/F(3,i);
    end
    Ph(:,i) = atan2(imag(H_oi(:,i)),real(H_oi(:,i)));

end

if isempty(CLDpos) == 0
zfr = 1001*abs(H_oi).*exp(1i*Ph);
mf = idfrd(zfr,nom.logomega*2*pi,0);
[~,modes_index] = findpeaks(abs(H_oi));
else
zfr = 1001*abs(H_oi).*exp(1i*-Ph);
```

```
mf = idfrd(zfr,nom.logomega*2*pi,0);
[~,modes_index] = findpeaks(abs(H_oi));
end
%% Calculate energies and loss factors at resonances

% if isempty(CLDpos) == 0

en_tot = zeros(length(modes_index),1); %vector to store total strain energy of beam
en_cld = zeros(nElem,length(modes_index)); %vector to store strain energy of CLD elements
en_bb = zeros(nElem,length(modes_index)); %vector to store strain energy of beam elements
en_p = zeros(nElem,length(modes_index)); %vector to store strain energy of piezo elements
lossfac = zeros(size(en_tot));

for i = 1:length(modes_index)
    j = modes_index(i);
    w = nom.logomega(j)*2*pi;
    [EI_CLD, ~] = rku(beam, visc, cl, p, G_star(j), Gprime(j), G_pp(j));
    u = U(:,j); %displacement at resonance freq
    cldindex = find(vElements);

    for k = 1:nElem
    n1 = k; %starting node
    n2 = k+1; %end node


    [K_bb, M_bb, K_CLD, M_CLD, K_p, M_p] = ElemMat(beam,visc,cl, piez, Ls(k), EI_CLD); %get all the elememtal matrices


    if vElements(k) == 1 %check whether element is CLD
        Kelem = K_CLD; %elastic stiffness matrix for CLD element
        Melem = M_CLD; %mass matrix for CLD element
        en_cld(k,i) = 0.5*u(n1*2-1:n2*2)'*Kelem*u(n1*2-1:n2*2);
        en_bb(k,i) = 0;
        en_p(k,i) = 0;
    elseif sElements(k) == 1 %check whether element is piezo
        Kelem = K_p; %stiffness matrix for piezo
        Melem = M_p; %mass matrix for piezo element
        en_p(k,i) = 0.5*u(n1*2-1:n2*2)'*Kelem*u(n1*2-1:n2*2);
        en_bb(k,i) = 0;
        en_cld(k,i) = 0;
    else
        Kelem = K_bb; %elastic stiffness matrix for base beam
        Melem = M_bb; %mass matrix for base beam
        en_bb(k,i) = 0.5*u(n1*2-1:n2*2)'*Kelem*u(n1*2-1:n2*2);
        en_cld(k,i) = 0;
```

```
        en_p(k,i) = 0;
    end

    if n1 == 1  %apply clamped boundary condition to first node
        Kelem(1:ms.nDofs,:) = zeros(ms.nDofs,ms.nDofs*2);
        Kelem(:,1:ms.nDofs) = zeros(ms.nDofs*2,ms.nDofs);
        Kelem(1:ms.nDofs,1:ms.nDofs) = eye(ms.nDofs);
        Melem(1:ms.nDofs,:) = zeros(ms.nDofs,ms.nDofs*2);
        Melem(:,1:ms.nDofs) = zeros(ms.nDofs*2,ms.nDofs);
        Melem(1:ms.nDofs,1:ms.nDofs) = eye(ms.nDofs);

    end
    K_sys(n1*ms.nDofs-(ms.nDofs-1):n2*ms.nDofs,n1*ms.nDofs-(ms.
       nDofs-1):n2*ms.nDofs) = K_sys(n1*ms.nDofs-(ms.nDofs-1):n2*
       ms.nDofs,n1*ms.nDofs-(ms.nDofs-1):n2*ms.nDofs)+ Kelem;
    M_sys(n1*ms.nDofs-(ms.nDofs-1):n2*ms.nDofs,n1*ms.nDofs-(ms.
       nDofs-1):n2*ms.nDofs) = M_sys(n1*ms.nDofs-(ms.nDofs-1):n2*
       ms.nDofs,n1*ms.nDofs-(ms.nDofs-1):n2*ms.nDofs) + Melem;

    end
    en_tot(i) = sum(en_p(:,i))+sum(en_bb(:,i))+sum(en_cld(:,i));
    if isempty(CLDpos) == 0
        %lossfac(i) = abs(en_cld(cldindex,i))*Eta(j)/abs(en_tot(i
           ));
        lossfac(i) = abs(sum(en_cld(:,i)))*Eta(j)/abs(en_tot(i));
    else
        lossfac = [];
    end
    if i == 2 %saves K and M at 2nd mode for state space model
        Kres2 = K_sys;
        Mres2 = M_sys;
    end
end

% else
%     lossfac = [];
%     en_tot = [];
%     en_cld = [];
% end
%% Modal decomposition and control implementation

if ~isempty(piezopos)

[Phi, omega2] = eigs(Kres2, Mres2, ms.nModes+2, 'smallestabs');
omega2 = abs((omega2));
omega = sqrt(diag(omega2));

if n_cld ~= 0
Phi = abs(Phi(:,3:end)); %get rid of rigid body modes
else
Phi = Phi(:,3:end);
```

```
end
omega2 = omega2(3:end, 3:end);


Phi = Phi/(Phi'*M_sys*Phi); %normalize modeshapes w.r.t. mass matrix
%Piezo inputs and outputs;
[intS,~] = shapeFunctions(); %get intergral of shape function
z = beam.h/2+piez.h; %effective height

%sensor equations
H = 1e11; %sensor gain
d31 = -180e-12;                                   % Piezo coupling d
s11 = 16.1e-12;
e31 = d31/s11;                                    % Piezo coupling e
w = beam.w;                                     % width of beam
S = - H*z*e31*w*intS;


%actuator equations
[~,intG] = shapeFunctions();
Ep = piez.E;
d31 =  -180e-12;
w = piez.w;
zbar = (piez.h+beam.h)/2;
G = Ep*d31*w*zbar*[0 -1 0 1]';%intG';

%External force input
Bext = zeros(nNodes*ms.nDofs,1);
if ms.tipforce == true
    Bext(end-1) = 1;
else
    Bext(3) = 1;
end

%modal damping matrix

Cmodal = 2*beam.zeta*sqrt(omega2);

%measurement and interpolation
height = ms.mesheight(1);
pos = zeros(1,nNodes);

for i = 1:length(Ls)+1

    if i == 1
        pos(i) = 0;
    end

```

```
    pos(i) = sum(Ls(1:(i-1)));

end

diff = pos-height;
lowerNodes = find(diff<0);
interpNodes = [lowerNodes(end), lowerNodes(end)+1];
interpEl = interpNodes(1);
%natural coordinate alpha
alpha = height - pos(interpNodes(1));
N1 = [1, alpha, alpha^2, alpha^3];
Aint = [1 0 0 0; 0 1 0 0; 1 Ls(interpEl) Ls(interpEl)^2 Ls(
   interpEl)^3; 0 1 2*Ls(interpEl) 3*Ls(interpEl)^2];
Ainv = inv(Aint);
N = N1*Ainv;
Cmeas = zeros(1,nNodes*ms.nDofs);
Cmeas(1, interpNodes(1)*2-1:interpNodes(1)*2+2) = N;




%Voltage input B and output C matrices

nsElements = length(piezopos)*piez.elemP; %number of smart
   elements
Cs = zeros(length(piezopos),nNodes*ms.nDofs);
Bg = zeros(nNodes*ms.nDofs,length(piezopos));
indx = find(sElements);

for i = 1:length(piezopos)
    for k = 1:piez.elemP
        el = indx((i-1)*piez.elemP + k);
        n1 = el;
        Bg(n1*2-1:n1*2+2,i) = Bg(n1*2-1:n1*2+2,i) + G;
        Cs(i,n1*2-1:n1*2+2) = Cs(i,n1*2-1:n1*2+2) + S;

    end

end

%create state-space model

A = [zeros(ms.nModes), eye(ms.nModes); -omega2, -Cmodal];

B = [zeros(ms.nModes, n_piezo+1); Phi'*Bext, Phi'*Bg];

C = [Cmeas*Phi, zeros(1,ms.nModes); Cs*Phi, zeros(n_piezo, ms.
   nModes)];

sys = ss(A,B,C,[]);

```

```
%Apply PPF feedback

if n_piezo == 0
    ms.fb = false;
end


if ms.fb == true
    [~,wpeak] = hinfnorm(sys(1,1));
    %wc = wpeak;
    wc = 120*2*pi;
    zetac = 0.2;
    kc =1;

    PPF = tf(kc*wc^2,[1 2*zetac*wc wc^2]);
    PPF = -PPF*eye(n_piezo);                                    % SISO PPF for every patch (just to test)

    sys_fb = feedback(sys,PPF,[2:1+n_piezo],[2:1+n_piezo],1); % Same system as before, only with ppf

end

else
    sys_fb = [];
    sys = [];
end
end
```

C.2 Calculate element lengths for FEM model

```
function [Ls,sElements, vElements] = getLength(beam, ms, piez, visc, CLDpos, piezopos, visco, pie, patchlengths)
    nPatches = length(piezopos);    % Number of piezo patches
    nCLD = length(CLDpos); %Number of CLD patches
    ntot = nPatches + nCLD; %total number of patches (smart and passive)
    nsElementsP = piez.elemP;     % Number of smart elements per patch
    nsElements = nPatches*nsElementsP; % Number of smart elements in total
    nvElementsP = visc.n; %number of viscoelastic elements per CLD patch
    nvElements = nCLD*nvElementsP; %number of viscoelastic elements in total
    L = beam.L; %total length of the beam

    %define gaps, these are the space between the smart elements, both
```

```
    %under and above them -> the actual beam elements
    if ~isempty(piezopos) && isempty(CLDpos) %case when there are smart elements but no CLD elements
        ngaps = nPatches+1;                              % Number of gaps in theory
        gaps = zeros(1,ngaps);

        for i = 1:ngaps% Get the length of every gap (between the patches)
            if i == 1                          % The first gap
                gaps(i) = piezopos(i)*L;
            elseif i <= nPatches                          % The rest of the gaps
                gaps(i) = piezopos(i)*L-(sum(gaps(1:i))+(i-1)*piez.L);
            else
                gaps(i) = L-(sum(gaps(1:i))+(i-1)*piez.elemL*nsElementsP);
            end
        end

        % Catch some errors here already
        if sum(gaps)+nPatches*piez.elemL*nsElementsP - L > 0
            error('Gaps are not correct (do not sum up to total length of beam)')
        end
        for i = 1:length(gaps)
            if gaps(i) < 0
                error('Patches are too close together! (They overlap)')
            end
        end

        nGapElements = ceil(gaps/(ms.LElem*L)); % Get number of elements per gap

        gelementLengths = cell(ngaps,1);
           % Intermediate cell array containing lengths of elements in gaps
        for i = 1:ngaps
            elementL = gaps(i)/nGapElements(i); %length of the gap divided by the number of elements per gap
            gelementLengths{i} = ones(1,nGapElements(i))*elementL; %vector with the length of each element in the gap
        end

        pelementLengths = cell(nPatches,1);   %Intermediate cell array containing length of piezo element lengths
        for i = 1:nPatches
```

```
            elementL = piez.elemL; %length of the element is length of the piezoelectric patch element
            pelementLengths{i} = ones(1,piez.elemP)*elementL; % vector wit the lengths of piezo patch elements
        end

        Ls = []; %create a vector to store the element lengths in
        sElements = []; %create a vector to identify which elements are smart

        for i = 1:nPatches+1
            if i <= nPatches
                Ls = [Ls,gelementLengths{i},pelementLengths{i}];
                sElements = [sElements,zeros(1,length(gelementLengths{i})),ones(1,length(pelementLengths{i}))];
            else
                Ls = [Ls,gelementLengths{i}];
                sElements = [sElements,zeros(1,length(gelementLengths{i}))];
            end
        end
        vElements = zeros(1,length(Ls)); %create a zero vector since there no CLD elements in this case
        if round(sum(Ls) - L,4) > 0
            error('Ls is not correct! (not the same as L')
        end
        if sum(sElements) - nsElements > 0
            error('sElements is incorrect!')
        end


    elseif ~isempty(CLDpos) && isempty(piezopos) %case when there are CLD elements but no smart elements
        ngaps = nCLD+1;                         % Number of gaps in theory
        gaps = zeros(1,ngaps);

        for i = 1:ngaps% Get the length of every gap (between the patches)
            if i == 1                  % The first gap
                gaps(i) = CLDpos(i)*L;
            elseif i <= nCLD                         % The rest of the gaps
                gaps(i) = CLDpos(i)*L-(sum(gaps(1:i))+(i-1)*visc.elemL*nvElementsP);
            else
                gaps(i) = L-(sum(gaps(1:i))+(i-1)*visc.elemL*nvElementsP);
            end
        end
```

```
    % Catch some errors here already
    if sum(gaps)+nCLD*visc.elemL*nvElementsP - L > 0
        error('Gaps are not correct (do not sum up to total length of beam)')
    end
    for i = 1:length(gaps)
        if gaps(i) < 0
            error('Patches are too close together! (They overlap)')
        end
    end

    nGapElements = ceil(gaps/(ms.LElem*L)); % Get number of elements per gap

    gelementLengths = cell(ngaps,1);          % Intermediate cell array containing lengths of elements in gaps
    for i = 1:ngaps
        elementL = gaps(i)/nGapElements(i); %length of the gap divided by the number of elements per gap
        gelementLengths{i} = ones(1,nGapElements(i))*elementL; %vector with the length of each element in the gap
    end

    pelementLengths = cell(nCLD,1);    %Intermediate cell array containing length of piezo element lengths
    for i = 1:nCLD
        elementL = visc.elemL; %length of the element is length of the piezoelectric patch element
        pelementLengths{i} = ones(1,visc.n)*elementL; %vector wit the lengths of piezo patch elements
    end

    Ls = []; %create a vector to store the element lengths in
    vElements = []; %create a vector to identify which elements are viscoelastic
    for i = 1:nCLD+1
       if i <= nCLD
           Ls = [Ls,gelementLengths{i},pelementLengths{i}];
           vElements = [vElements,zeros(1,length(gelementLengths{i})),ones(1,length(pelementLengths{i}))];
       else
           Ls = [Ls,gelementLengths{i}];
           vElements = [vElements,zeros(1,length(gelementLengths{i}))];
       end
    end
```

```
        sElements = zeros(1,length(Ls)); %create a zero vector since there are no smart elements in this case
        if round(sum(Ls) - L,4) > 0
            error('Ls is not correct! (not the same as L')
        end
        if sum(vElements) - nvElements > 0
            error('sElements is incorrect!')
        end

    elseif ~isempty(piezopos) && ~isempty(CLDpos)
        ngaps = ntot+1; %total number of gaps
        gaps = zeros(1,ngaps);


        for i = 1:ngaps% Get the length of every gap (between the patches)
            if i == 1                   % The first gap
                gaps(i) = (visco(i)+pie(i))*L;

            elseif i <= ntot                      % The rest of the gaps

                gaps(i) = (visco(i)+pie(i))*L-(sum(gaps(1:i))+sum(patchlengths(1:(i-1))));

            else
                gaps(i) = L-(sum(gaps(1:i-1))+sum(patchlengths(1:(i-1)))); %the last gap
            end
        end

        % Catch some errors here already
        if round(sum(gaps)+ sum(patchlengths) - L,4) > 0
            error('Gaps are not correct (do not sum up to total length of beam)')
        end
        for i = 1:length(gaps)
            if gaps(i) < 0
                error('Patches are too close together! (They overlap)')
            end
        end

        nGapElements = ceil(gaps/(ms.LElem*L)); % Get number of elements per gap

        gelementLengths = cell(ngaps,1); % Intermediate cell array containing lengths of elements in gaps
        for i = 1:ngaps
```

```
            elementL = gaps(i)/nGapElements(i); %length of the gap divided by the number of elements per gap
            gelementLengths{i} = ones(1,nGapElements(i))*elementL; %vector with the length of each element in the gap
        end

        pelementLengths = cell(ntot,1);   %Intermediate cell array containing length of piezo element lengths

        for i = 1:ntot
            if patchlengths(i) == piez.L
            elementL = piez.elemL; %length of the element is length of the visco patch element
            pelementLengths{i} = ones(1,piez.elemP)*elementL; %vector wit the lengths of visco patch elements
            else
            elementL = visc.elemL;
            pelementLengths{i} = ones(1,visc.n)*elementL; %vector with the length of visco elements
            end
        end


        Ls = []; %create a vector to store the element lengths in
        sElements = []; %create a vector to identify which elements are smart
        vElements = []; %create a vector to identify which elements are viscoelastic
        for i = 1:ntot+1
           if i <= ntot
               Ls = [Ls,gelementLengths{i},pelementLengths{i}];
               if patchlengths(i) == piez.L
               sElements = [sElements,zeros(1,length(gelementLengths{i})),ones(1,length(pelementLengths{i}))];
               vElements = [vElements,zeros(1,length(gelementLengths{i})),zeros(1,length(pelementLengths{i}))];
               else
               sElements = [sElements,zeros(1,length(gelementLengths{i})),zeros(1,length(pelementLengths{i}))];
               vElements = [vElements,zeros(1,length(gelementLengths{i})),ones(1,length(pelementLengths{i}))];
               end
           else
           Ls = [Ls,gelementLengths{i}];
           sElements = [sElements,zeros(1,length(gelementLengths{i}))];
```

```
            vElements = [vElements,zeros(1,length(gelementLengths{i}))];
            end
        end


        if round(sum(Ls) - L,4) > 0
            error('Ls is not correct! (not the same as L')
        end
        if (sum(sElements)+sum(vElements)) - (nvElements+nsElements) > 0
            error('sElements is incorrect!')
        end

    else % case when there are no smart of visco element (bare beam)
        nElements = 1/ms.LElem;
        Ls = ones(1,nElements)*L/nElements;
        sElements = zeros(length(Ls));
        vElements = zeros(length(Ls));
        end


    %sElements = find(sElements);
    %sElements = reshape(sElements,piez.elemP,[]);
    %vElements = find(vElements);


end
```

C.3 Plotting and results

```
%clear all

%bode plot options

plotoptions = bodeoptions;
plotoptions.Title.String = '';
plotoptions.Title.Interpreter = 'latex';
plotoptions.XLabel.Interpreter = 'latex';
plotoptions.YLabel.Interpreter = 'latex';
plotoptions.XLabel.FontSize = 13;
plotoptions.YLabel.FontSize = 13;
plotoptions.FreqUnits = 'Hz';
plotoptions.grid = 'on';
%plotOptions.PhaseWrapping = 'off';
plotoptions.XLim = {[1 10e3]};

%Base beam parameters
beam.L = 0.277; %length of beam [m]
beam.w = 0.04; %width of beam [m]
```

```
beam.h = 0.0016; %height of beam [m]
beam.E = 70e9; %elasticity modulus [Pa]
beam.A = beam.w*beam.h; %cross section of beam [m^2]
beam.I = beam.w*beam.h^3/12; %beam moment of inertia [m^4]
beam.rho = 2700; %density [kg/m^3]
beam.mu = 0.334; %Poisson ratio of beam
beam.zeta = 0.01; %modal damping ratio of the beam
beam.m = beam.rho*beam.A*beam.L; %mass of the base beam [kg]

%Piezo patch parameters
piez.L = 0.22*beam.L; %length of the piezo patch [m]
piez.rho = 7800; %density of patch [kg/m^3]
piez.h = 0.0005; %height of the piezo patch [m]
piez.w = 0.035; %width of the patch [m]
piez.E = 52e9; %stiffness of the beam [Pa]
piez.A = piez.w*piez.h; %cross sectional area of patch [m^2]
piez.I = (piez.w*piez.h^3)/12 + piez.w*piez.h*(0.25*(piez.h+beam.h)^2);
piez.elemP = 3; %number of piezo elements per patch%moment of inertia of patch and beam
piez.elemL = piez.L/piez.elemP; %length of piezo element
piez.m = piez.A*piez.L*piez.rho;

%Viscoelastic patch parameters
visc.n = 1; %no of visc elements per patch
visc.rho = 1.011e3; %density of viscoelastic material [kg/m^3]
visc.w = 0.035; %width of visco [m]
visc.h = 0.000127; %height of visco [m]
visc.A = visc.w*visc.h; %cross section of viscoleastic material [m^2]
visc.I = visc.w*visc.h^3/12; %moment of inertia of visc [m^4]
visc.E = 3e9;%placeholder for complex modulus
visc.L = 0.40*beam.L; %length of viscoleastic beam element [m]
visc.m = visc.A*visc.L*visc.rho; %mass of viscoleastic patch [kg]
visc.G = 3e9; %placeholder for shear modulus [Pa]
visc.mu = 0.49; %poisson ratio
visc.elemL = visc.L/visc.n; %length of a CLD element [m]


%Constraining layer parameters
cl.n = visc.n; %number of constraining layer elements
cl.rho = beam.rho; %density of constraining layer [kg/m^3]
cl.w = visc.w; %width of constraining layer [m]
cl.h = visc.h*2; %height of constraining layer [m]
cl.L = visc.L; %length of constraining layer [m]
cl.E = beam.E; %E modulus of constraining layer [m]
cl.A = cl.w*cl.h; %Cross section of constraining layer [m^2]
cl.I = cl.w*cl.h^3/12; %Moment of inertia [m^4]
cl.m = cl.A*cl.L*cl.rho; % mass of constraining layer [kg]

%Model settings
```

```
ms.fb = true; %apply feeback
ms.nDofs = 2; %mnumber of dofs per node
ms.nModes = 4; %number of modes to be calculated
ms.mesheight = 0.2*beam.L; %place where we measure displacement
ms.LElem = 0.1; %preferred length of beam elements
ms.tipforce = false; %decide whether force is applied at tip or
    base
ms.modeshapes = false; %calculate mode shapes or not
ms.patchinput = false; %input is patch disturbance
ms.plotstrain = false; %plot strain energy distribution
ms.constG = false; %use constant G' instead of varying G'


CLDpos = {[],[0.2772]}; %Position of CLD patches x/L
piezopos = {[],[0.0475]}; %Position of Piezo patches x/L
%CLDpos = {[],[0.65], [0.43 0.65],[0.05 0.43 0.65]};
%piezopos = {[],[0.54], [0.54], [0.54]};
%CLDpos = {[]};
%piezopos = {[0.05 0.439 0.54 0.65],};
Legend = cell(size(CLDpos)); %store legend here
Lengend2 = cell(1,2*length(Legend)); %store legend for fb here
wpeak = cell(length(CLDpos),1); %store resonance peaks
wpeakfb = cell(1,length(CLDpos)); %store resonance peaks w/ fb
zeta = cell(size(wpeak)); %store damping ratio
zeta_fb = cell(size(wpeak)); %store damping ratio w/ fb
peakind = cell(size(zeta)); %store peak index here
nElem = zeros(length(CLDpos),1); %number of CLD elements
bodopt = bodeoptions;
bodopt.FreqUnits = 'Hz';
bodopt.XLim = {[1 1000]};
bodopt.MagUnits = 'dB';

%coverage = {['Piezo length: 10 %'],['Piezo length: 20 %'],['
    Piezo length: 30 %'],['Piezo length: 40 %'], ['Piezo length:
    50 %']};
fbsystems = cell(size(CLDpos)); %store damping ratios here w/ fb
ZETA = zeros(4,length(CLDpos)); %store CLD damping ratios
ms.mesheightcol = cell(size(CLDpos)); %measurement height for
    collocated control

for i = 1:length(CLDpos)
    ms.mesheightcol{i} = piezopos{i}*beam.L; %sensor collocated
        with actuator
    ms.mesheight = ms.mesheightcol{i}+0.01;
    [mf,sys,sys_fb, U, mode_index, nEl, H_oi, lossfac, en_tot,
        en_cld, en_bb] = batchbeam(beam,visc,cl,piez,ms,CLDpos{i},
        piezopos{i}); %calculate and solve FEM model
    nElem(i) = nEl;
    peakind{i} = mode_index;
    cldstr = string(CLDpos{i});
```

```
    %cldstr = string(coverage{i});
    pstr = string(piezopos{i});
    Legend{i} = join(['CLD position:' cldstr ';' 'Piezo position:
       ' pstr]);
    fbsystems{i} = sys_fb;
    %Legend{i} = join(['' cldstr]);
    if CLDpos{i} ~= 0
    ZETA(:,i) = lossfac(1:4)*0.5;
    end

    figure(1)  %plot system without fb
    hold on
    bode(mf,bodopt)
    grid on

    if ~isempty(sys) && ~isempty(sys_fb)

    figure(2) %plot system with fb
    hold on
    bod = bodeplot(gca,sys(1,1),sys_fb(1,1),plotoptions);
    [wn,zet] = damp(sys(1,1));
    wpeak{i} = wn;
    zeta{i} = zet;
    [wnfb,zetafb] = damp(sys_fb(1,1));
    wpeakfb{i} = wnfb;
    zeta_fb{i} = zetafb;

    end
end

 %zeta calculated from loss factor which was calculated with
    strain energies

figure(1)
legend(Legend,'Fontsize',14)
figure(2)
legend('Uncontrolled','PPF','Fontsize',12)

%% plot modeshapes for first three modes

if ms.modeshapes == true

v = cell(size(peakind));
nmodes = (1:3);
%get displacements at resonant freq (to plot mode shapes)
for i = 1:length(nmodes)

indx = peakind{1}(i); %gets the index of mode of interest
v{i} = real((U(:,indx)));
v{i} = v{i}(1:2:end)/beam.L;
figure(3)
```

```
hold on
plot(v{i})
Leg{i} = join(['Mode', string(i)]);


end
legend(Leg)
end

%% Section to plot strain energy distribution in the beam
if ms.plotstrain == true

%leg = zeros(3,1); %vector to contain legend
for i = 1:3

en = en_bb(:,i);
en = [en; 0];
x = (0:nElem)/nElem; %normalized beam length
xq = x(1):0.001:x(end);
yinterp = pchip(x,en,xq);
yinterp = yinterp/max(yinterp);
xcld1 = 0.425;
xcldend = (0.15)+xcld1;
xpiez = 0.325;
xpiezend = 0.1 + 0.325;
ptchidxp = (xq >=xpiez) & (xq <=xpiezend);
ptchidx = (xq >= xcld1) & (xq <=xcldend);
Leg{i} = join(['Mode', string(i)]);
figure
plot(xq,yinterp)
hold on
patch([xq(ptchidx) fliplr(xq(ptchidx))], [yinterp(ptchidx) zeros(size(yinterp(ptchidx)))], [0.6 0.4 0.9], 'FaceAlpha',0.3, 'EdgeColor','none')
patch([xq(ptchidxp) fliplr(xq(ptchidxp))], [yinterp(ptchidxp) zeros(size(yinterp(ptchidxp)))], [0.01 0.01 0.1], 'FaceAlpha',0.3, 'EdgeColor','none')
title('Strain energy distribution')
xlim([0 1])
xlabel('Normalized beam length')
ylabel('Normalized strain energy')
legend(Leg{i},'CLD patch','Piezo patch')

end
end
```